④

David Taylor Research Center

Bethesda, MD 20084–5000

Electrolysis Bubble Noise in Small-Scale Tests of a Seawater MHD Thruster

by
Kenneth E. Tempelmeyer
Secretary of the Navy Fellow, U.S Naval Academy, and
Consultant, David Taylor Research Center

DTIC
ELECTE
OCT 12 1990
S E D

AD-A227 548

MAJOR DTRC TECHNICAL COMPONENTS

CODE 011 DIRECTOR OF TECHNOLOGY, PLANS AND ASSESSMENT

12 SHIP SYSTEMS INTEGRATION DEPARTMENT

14 SHIP ELECTROMAGNETIC SIGNATURES DEPARTMENT

15 SHIP HYDROMECHANICS DEPARTMENT

16 AVIATION DEPARTMENT

17 SHIP STRUCTURES AND PRO゙ ᴇCTION DEPARTMENT

18 COMPUTATION, MATHEMATICS & LOGISTICS DEPARTMENT

19 SHIP ACOUSTICS DEPARTMENT

27 PROPULSION AND AUXILIARY SYSTEMS DEPARTMENT

28 SHIP MATERIALS ENGINEERING DEPARTMENT

DTRC ISSUES THREE TYPES OF REPORTS:

1. **DTRC reports, a formal series,** contain information of permanent technical value. They carry a consecutive numerical identification regardless of their classification or the originating department.

2. **Departmental reports, a semiformal series,** contain information of a preliminary, temporary, or proprietary nature or of limited interest or significance. They carry a departmental alphanumerical identification.

3. **Technical memoranda, an informal series,** contain technical documentation of limited use and interest. They are primarily working papers intended for internal use. They carry an identifying number which indicates their type and the numerical code of the originating department. Any distribution outside DTRC must be approved by the head of the originating department on a case-by-case basis.

REPORT DOCUMENTATION PAGE

1a. REPORT SECURITY CLASSIFICATION	1b. RESTRICTIVE MARKINGS
Unclassified	

2a. SECURITY CLASSIFICATION AUTHORITY	3. DISTRIBUTION/AVAILABILITY OF REPORT
2b. DECLASSIFICATION/DOWNGRADING SCHEDULE	Approved for public release; distribution is unlimited.

4. PERFORMING ORGANIZATION REPORT NUMBER(S)	5. MONITORING ORGANIZATION REPORT NUMBER(S)
DTRC—90/30	

6a. NAME OF PERFORMING ORGANIZATION	6b. OFFICE SYMBOL (If applicable)	7a. NAME OF MONITORING ORGANIZATION
David Taylor Research Center	Code 2712	

6c. ADDRESS (City, State, and ZIP Code)	7b. ADDRESS (City, State, and ZIP Code)
Bethesda, MD 20084-5000	

8a. NAME OF FUNDING/SPONSORING ORGANIZATION	8b. OFFICE SYMBOL (If applicable)	9. PROCUREMENT INSTRUMENT IDENTIFICATION NUMBER
	DTC C0113	

8c. ADDRESS (City, State, and ZIP Code)	1c. SOURCE OF FUNDING NUMBERS			
	PROGRAM ELEMENT NO.	PROJECT NO.	TASK NO.	WORK UNIT ACCESSION NO.
DTRC Bethesda, Maryland 20084-5000	62936N	1-2712-131	ZF66412001	500540

11. TITLE (Include Security Classification)
Electrolysis Bubble Noise in Small-Scale Tests of a Seawater MHD Thruster

12. PERSONAL AUTHOR(S)
Kenneth E. Tempelmeyer

13a. TYPE OF REPORT	13b. TIME COVERED	14. DATE OF REPORT (YEAR, MONTH, DAY)	15. PAGE COUNT
Final	FROM____ TO____	September 1990	48

16. SUPPLEMENTARY NOTATION
This work was a cooperative effort with the United States Naval Academy, Annapolis, Maryland 21402.

17. COSATI CODES			18. SUBJECT TERMS (Continue on reverse if necessary and identify by block number)
FIELD	GROUP	SUB-GROUP	Acoustic noise, Bubble formation, Electrolysis, Magnetohydrodynamics, Noise, Seawater

19. ABSTRACT (Continue on reverse if necessary and identify by block number)

Sound pressure levels were measured during the electrolysis process of seawater in a magnetohydrodynamic-type channel, but without an applied magnetic field. The test configuration was a small-scale version of a seawater magnetohydrodynamic (MHD) thruster and the test conditions were similar to those which might occur in an undersea MHD-powered vessel. The electrolysis of sea water at current densities up to 0.3 $A/cm^{(2)}$ produced broad-band noise at frequencies above 2 kHz and up to 20 kHz. Most of the acoustic energy was in the 2 to 6 kHz range. A few noise peaks were superimposed upon the broad-band noise. The most significant of these appeared to be associated with transverse standing waves in the flow channel.

The increased noise levels resulted from the oscillation of hydrogen bubbles produced during electrolysis as these hydrogen bubbles (1) detach from the electrode surface and (2) coalesce, forming larger bubbles. The test data suggest that bubble coalescence is the principal noise source. Bubble diameter, inferred from the noise data, appears to be in the range of 0.075 to 0.15 mm. The bubble noise was relatively easy to measure and to discern from test facility noise and flow-induced noises. Some comparisons with previous noise measurements are made and various factors that influence the bubble noise are outlined. Keywords: Underwater (?) ... hydrodynamics (RH)

20. DISTRIBUTION/AVAILABILITY OF ABSTRACT	21. ABSTRACT SECURITY CLASSIFICATION
[X] UNCLASSIFIED/UNLIMITED ☐ SAME AS RPT ☐ DTIC USERS	Unclassified

22a. NAME OF RESPONSIBLE INDIVIDUAL	22b. TELEPHONE (Include Area Code)	22c. OFFICE SYMBOL
Dr. Samuel H. Brown	(301)-267-2146	Code 2712

CONTENTS

FIGURES

TABLES

SYMBOLS

C	Speed of sound
C_e	Wave speed
c_p	Specific heat at constant pressure
c_v	Specific heat at constant volume
d	Width of electrode
d_{bubble}	Bubble diameter
E	Electric field
F	Faraday's constant
f	Frequency
f_0	Resonant frequency of oscillating bubble
f_n	Frequency of standing wave
I	Current
j	Current density
L	Channel or electrode length
l	Channel transverse length
n	Integer
P	Pressure
p_0	Fluid pressure
R	Gas constant
r_b	Bubble radius
S	Specific gravity
T	Temperature
t	Time
u	Velocity
u_∞	Freestream velocity
V	Voltage or volume
V_0	Initial volume
$\dot{V}$	Volume flow rate
w	Spacing between electrodes
β	Void fraction
γ	Specific heat ratio
ρ	Density
ω_0	Angular frequency

ABBREVIATIONS

A	Amperes
ac	Alternating current
B&K	Bruel & Kaer
DARPA	Defense Advanced Research Projects Agency
DTRC	David Taylor Research Center
dB	Decibels
dc	Direct current
F	Faraday (96,487 coulombs)
FFT	Fast Fourier transform
Hz	Hertz (cycles per second)
kHz	Kilohertz
MHD	Magnetohydrodynamic
μPa	Micropascals
Pa	Pascals
SPL	Sound pressure level
SW	Standing wave
V	Volts

ABSTRACT

Sound pressure levels were measured during the electrolysis process of seawater in a magnetohydrodynamic-type channel, but without an applied magnetic field. The test configuration was a small-scale version of a seawater magnetohydrodynamic (MHD) thruster and the test conditions were similar to those which might occur in an undersea MHD-powered vessel. The electrolysis of sea water at current densities up to 0.3 A/cm^2 produced broad-band noise at frequencies above 2 kHz and up to 20 kHz. Most of the acoustic energy was in the 2- to 6-kHz range. A few noise peaks were superimposed upon the broad-band noise. The most significant of these appeared to be associated with transverse standing waves in the flow channel.

The increased noise levels resulted from the oscillation of hydrogen bubbles produced during electrolysis as these hydrogen bubbles (1) detach from the electrode surface and (2) coalesce, forming larger bubbles. The test data suggest that bubble coalescence is the principal noise source. Bubble diameter, inferred from the noise data, appears to be in the range of 0.075 to 0.15 mm. The bubble noise was relatively easy to measure and to discern from test facility noise and flow-induced noises. Some comparisons with previous noise measurements are made and various factors that influence the bubble noise are outlined.

ADMINISTRATIVE INFORMATION

ACKNOWLEDGMENTS

INTRODUCTION

The acceleration of electrically conducting fluids by crossed electric and magnetic fields (i.e. magnetohydrodynamic or MHD propulsion) has been proposed and investigated for many years. Commercially available liquid-metal pumps utilize this concept, but MHD propulsion has had limited success in other applications. One problem limiting the successful application of MHD thrusters has been the inability to produce the high magnetic field strengths needed. The performance of the device is related to the electrical conductivity of the fluid and the magnetic field strength; thus high magnetic fields are essential when the conductivity is low.

Because seawater is an electrical conductor, the application of this concept for ship propulsion has been repeatedly suggested over the past three decades. (See refs. 1 through 6 for example.) Seawater MHD thrusters have not been pursued in the past because of the poor performance which would result at low magnetic fields. However, with the advent of superconducting magnets, which can produce fields of 6 to 10 tesla, the application of MHD thrusters for seawater becomes more feasible. As a result, interest in this propulsion concept is increasing at several naval laboratories and at the Defense Advanced Research Projects Agency (DARPA). Furthermore, the Japanese have reported on an MHD ship propulsion program.[7,8] Their work has apparently resulted in the construction of a prototype which is reported to have two MHD thrusters, each producing a Lorentz force of 8000 newtons with a 4 tesla superconducting magnet installed in a vessel having a displacement of about 150 tons.*

Recent interest in this ship propulsion concept is also stimulated in part by the expectation that an MHD thruster would be quieter than conventional methods of providing mechanical power to shafts and propellers. The reason for the interest in undersea MHD vehicle propulsion is obvious — perhaps too obvious, since the news media speculated and widely reported that the Soviet *Victor* Class submarine may have utilized MHD propulsion units.[9,10] This speculation appeared to be based on photographs that show a small pod on the stern of the vessel. This pod was presumed to contain the MHD thruster unit. This speculation has no apparent basis in fact; the pod appears too small to contain any useful MHD propulsion unit. In any case, the prospect of quieter operation provides a strong incentive to consider propellerless MHD propulsion units, since it would eliminate not only the noise associated with propeller cavitation but also the mechanical vibrations and noises associated with a gear reduction box and a rotating shaft.

The MHD process in seawater is not noise free, however. As an electric current passes through the water, electrolysis occurs. In the MHD thruster, hydrogen bubbles are produced at the cathode and chlorine at the anode. Depending upon the anode material, the chlorine generated at the anode can be very quickly hydrolyzed, producing hypochlorite and hydrogen.[11] This generates additional hydrogen bubbles. Since the bubbles may oscillate as they leave the electrode surfaces or as they coalesce, they can serve as a noise source functioning in an ideal sense as a linear harmonic oscillator. To evaluate the feasibility of seawater MHD thrusters, the noise potential of the electrolysis process should be examined both experimentally and analytically.

---

*Seizo Motora, "Research and Development of Superconducting Electromagnetic Propulsion Ships," Japan Foundation of Shipbuilding Advancement (unpublished communication).

The David Taylor Research Center (DTRC) has been analytically studying the application of MHD thrusters for ship propulsion over the past several years.[12]* To support this activity, an experimental program to test the electrical characteristics of an MHD thruster was started at the U.S. Naval Academy in cooperation with DTRC.[13] The purposes of these tests were (1) to investigate the electrolysis process in an MHD channel (without an applied magnetic field), (2) to observe the bubble formation, and (3) to make preliminary measurements of the bubble noise. Reference 13 reports on the electrical characteristics of seawater electrolysis in an MHD channel. This report provides information concerning (1) bubble formation and dynamics and (2) the noise spectrum of a small-scale seawater MHD channel. The tests were conducted without a magnetic field, and the seawater was simulated by using commercially available salt compounds.

BACKGROUND

The mechanisms of underwater noise were thoroughly discussed by Ross[14] over a decade ago. The work, which was supported by the Office of Naval Research, summarizes the causes of bubble noise from several sources such as cavitation, entrainment of air by waves and/or wakes, and gas discharges into water. The electrolysis of seawater in an MHD thrust unit provides another mechanism for bubble generation and bubble noise, which has not been extensively studied.

In its simplest form, the electrolysis of water results in the generation of chlorine gas at the anode and hydrogen gas at the cathode by the reactions:

$$\text{Anode} \quad 2Cl^- \rightarrow Cl_2 + 2e^- \tag{1}$$

$$\text{Cathode} \quad 2e^- + 2H_2O \rightarrow H_2 + 2(OH)^- \tag{2}$$
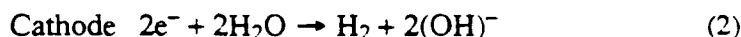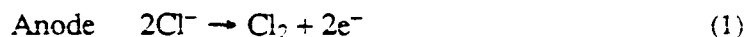
More complicated electrode reactions can also occur, depending upon the electrode materials used and the level of current. Bennett[15] states that chlorine generated at the anode will very quickly be hydrolyzed and H_2 generated by the reactions:

$$2Cl^- \rightarrow Cl_2 + 2e^- \tag{3}$$

$$Cl_2 + H_2O \Leftrightarrow HClO + Cl^- + H^+ \tag{4}$$

$$HClO \Leftrightarrow ClO^- + H^+ \tag{5}$$

$$2H^+ + 2e \rightarrow H_2 \tag{6}$$
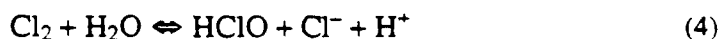
The amount of hydrogen gas produced at the cathode can be calculated quite simply, since one hydrogen molecule is produced for every two electrons. Measurement of the electrolysis current was used as an early means of determining Avogadro's Number. One faraday of charge, F, (96,487 coulombs) will produce one mole or 1.008 g of hydrogen, assuming all of the H_2 generated is in the form of H_2 gas. As a result, it can be shown that the volumetric production of H_2 is:

$$\dot{V} = \left(\frac{I}{F}\right) \times \left(\frac{RT}{2P}\right) \tag{7}$$

if the H_2 generated is treated as a perfect gas.

*Also D. Bagley, private communication (Sept 1989).

7" . amount of H_2 produced at the anode by hydrolyzation of Cl_2 is more difficult to estimate because the rate of this process (Eqs. 3–6) could not be determined. With certain anode materials such as aluminum, bubbles are observed on the anode, but they are not nearly as abundant as the H_2 bubbles generated at the cathode. With other anode materials such as copper and stainless steel, few bubbles were observed on the anode.

In any event, as an H_2 bubble is generated at the wall, it passes through the shape changes shown in Fig. 1a. It leaves the wall as a flattened spheroid (stage 3) and begins to oscillate (stage 4) until it reaches an equilibrium spherical shape. The oscillation stage generates noise which radiates as a simple monopole source. Monopole noise sources are essentially omnidirectional. Thus the noise is propagated both upstream and downstream from the MHD channel.

Observation of the bubble formation (Tempelmeyer[13]) clearly demonstrated that small-diameter bubbles (probably less than 0.5 mm in diameter) are generated uniformly over the cathode and to a lesser degree with some anode materials. (Additional bubble size information during electrolysis, obtained photographically by Sides,[16] indicated that electrolysis bubbles may be still smaller.) The bubbles rise and move downstream in the electrode boundary layers under a balance of forces due to (1) shear in the boundary layer, (2) their natural buoyancy, and (3) their surface tension with the wall. If the electrodes are located on the vertical sidewalls of the channel (Fig. 2b), the bubbles rise due to their buoyancy but remain in the electrode sidewall boundary layer until they reach the top of the channel. As they rise, they are also convected downstream by the boundary-layer flow. When the bubbles were generated at a horizontal bottom wall (Fig. 2c), the hydrogen bubbles produced at the cathode rose through the boundary layer because of their buoyancy and moved into the free stream where they were more rapidly convected downstream. However, bubbles formed at the electrode and sidewall corner rose in the sidewall boundary layer and stayed close to the sidewall. As a result, many of these bubbles reached the top of the wall before moving out of the channel, and they formed small gas pockets at the corners of the upper wall (i.e. the channel ceiling).

Within the electrode boundary layers and in the free stream, the bubbles may coalesce, producing nonspherical shapes which oscillate and serve as noise sources, as depicted in Fig. 1b. Noise is also produced if the bubbles subdivide. However, observation of the bubble dynamics[13] suggests that this is not a dominant mechanism in the electrolysis process for these tests.

Minnaert[17] was the first to develop an expression for the resonant frequency of oscillating gas bubbles. He considered the bubble as a simple harmonic oscillator with no damping and with a bubble diameter small compared to the wavelength of the sound. The bubble acoustic model is represented by the expression

$$\frac{d^2V}{dt^2} = -(\omega_0)^2(V - V_0) ,$$ (8)

which, when solved for the resonant frequency of the bubble oscillation, gives

$$f_0 = \frac{w_0}{2\pi} \frac{1}{2\pi r_b} \sqrt{\frac{3\gamma p_0}{\varrho_0}} .$$ (9)

For a gas with a specific heat ratio of 1.4 in water, Eq. 9 can be written as

$$f_0 \simeq \frac{3.28}{r_b} \sqrt{p_0} \ , \tag{10}$$

where f_0 is the resonant frequency in hertz, r_b the bubble radius in meters and p_o is the water pressure. (Strasberg[18] has expanded this analytical model to include the effects of damping.) The Minnaert equation (Eq. 9) is widely used to determine the frequency of bubble noise in water and to relate the noise to bubble size.

Little direct information concerning bubble noise in an electrolysis of water could be found in the open literature. Richardson[19] summarizes some data on sound damping or attenuation of H_2 bubble noise during the electrolysis of water in a static cell having both plate and wire mesh electrodes. These data suggest the bubble noise occurred in a frequency range from 5 to 50 kHz, which, as will be shown later, is the same range of frequencies measured in the present tests. The information shown by Richardson also indicates that the noise is highly attenuated at frequencies over 20 kHz.

Some measurements of air bubble sizes in ocean water indicated that the bubbles are smaller than would be expected from bubble size measurement in fresh water.[20-24] While the cause of this effect is not fully understood, some evidence indicates that the bubble gas cavity may be coated with a film produced by biological material in the ocean. The composition, uniformity and thicknesses of the biological films are uncertain and highly variable. The reported results have focused on air bubbles entrained by wave action. These bubbles have small diameters and longer lifetimes than would be expected, which is attributed to an organic film coating.

If this effect exists, it would be more prevalent at the ocean's surface than at depth. Study of this biological coating effect on electrolysis bubbles is beyond the scope of the tests reported here, since simulated seawater was used in all tests, but this is a phenomenon which deserves further consideration.

TEST EQUIPMENT

WATER TABLE FACILITY AND FLOW CHANNELS

Bubble noise was measured using two water tables which produce a sheet of water having a specified depth. Wall guides were introduced to simulate a two-dimensional flow channel consisting of an intake nozzle, a constant area MHD channel, without magnetic induction (i.e., no B–field), and an exit diffuser (see Fig. 3). Bubble noise data were obtained for two basic channel configurations:

Open-Top Channel

Some long-duration durability tests on electrode materials were carried out using an open-top channel as reported in ref. 13. Bubble noise measurements were also made as a secondary effort during those tests. In this configuration, the electrodes made up the sidewalls of the channel as shown in Fig. 3. The bottom wall or floor was made of an insulating material, and a free water surface existed at the top. This configuration is acoustically complex. Its noise characteristics would be different from those of a linear closed channel

MHD seawater thruster being considered.[1-5]* Some data from the open-top channel configuration are included here for comparison. Figure 4 is a photograph of this configuration. The channel length was 12.7 cm; the spacing between the electrodes was 5 cm; and the depth of the water was 1.8 to 2.0 cm. The flow velocity for all of the open-channel tests reported here was about 47 cm/sec. The electrodes were made of materials commonly used in seawater electrolysis cells and produced by Eltech Corp. The electrical conductivity of the water was about 4.5 siemens per meter (S/m), and the electric currents for these tests were varied to above 6 A.

Closed Channel

Most of the bubble noise measurements were made with a constant-area, enclosed channel. When a completely closed channel configuration was used, the bottom surface of the channel served as the cathode, the top surface as the anode, and the sidewalls were made from nonconducting materials. This channel was fully submerged in the water flow. A photograph of the closed channel is shown in Fig. 5.

Aluminum electrodes were used in the closed channel, which was 13.8 cm long. The spacing between the electrodes was 3.7 cm, and the height of the electrodes was 3.4 cm. The conductivity of the water was maintained at 4.5 S/m, and the current was varied to over 10 A.

POWER SUPPLY AND INSTRUMENTATION

The electrodes were connected to a direct current (dc) power supply. Applied voltages ranged from 0 to 30 V; the corresponding current ranged from 0 to more than 10 A. Current and voltage measurements were made for each of the electrode pairs by applying various voltages up to the value which produced a current density of 0.2 to 0.3 A/cm^2. For a few tests, a battery power supply was used to determine if the measured sound pressures were in some way induced by the power supply.

Currents and voltages were measured with Fluke meters. The repeatability of the electrical measurements was well within 2%. Approximate values of the flow velocity were obtained from (1) a water flow meter in the water table and (2) by timing the passage of a small floating object in the MHD channel. Test velocities ranged from 0 up to about 70 cm/sec. The accuracy of the flow velocity measurement was no better than about ±10% of the values stated.

Sound pressure level measurements were made with a Bruel & Kaer (B&K) Hydrophone Model 8103. This was the smallest hydrophone probe available. It was 0.7 cm in diameter and protruded into the flow about 2 cm. The hydrophone is shown in Figs. 4 and 5 downstream of the electrolysis channel. Its position was varied both axially and laterally. While most of the sound pressure level measurements were made downstream of the channel in the exit diffuser, some upstream acoustic measurements were also made for comparative purposes. The frequency response of this hydrophone was flat up to about 100 kHz. It was used to measure sound at frequencies up to 50 kHz.

The output of the hydrophone was supplied to one of two B&K narrow-band frequency analyzers (either a Model 2515 or a Model 2032). The Model 2032 analyzer, used

---

to record most of the noise spectra presented here, also used a B&K Model 2635 charge amplifier to precondition the signal. Both analyzers statistically sampled the signal and then calculated the sound spectrum through a fast Fourier transform (FFT), displaying the spectrum over two or three decades of frequency up to 20 kHz for the Model 2515 and 25 kHz for the Model 2032. For most test points, from 200 to 4000 data averages were compiled by the analyzer in determining the spectrum. For the conditions of these tests, the FFT calculated spectrum did not change in any important way after 200 data samples were taken. In most instances, the test data were sampled and compiled in constant 32 Hz bandwidths. The analyzer was set up to measure the sound pressure level in pascals. A decibel scale is also shown on some plots. A value of 1 µPa was used in converting to the dB scale.

To record the noise spectrum at frequencies up to 50 kHz, a Real Time Systems, Inc. frequency divider was used in conjunction with the B&K Model 2032 frequency analyzer. This device uses a timing circuit to process the input signal and extend the frequency range of the analyzer. The accuracy of the Real Time System device was evaluated by generating signals of known frequency and analyzing them with and without the frequency divider. The device accurately divided the signal, providing confidence that the spectral data up to 50 kHz are reliable.

Spectra obtained with the Model 2515 analyzer were stored and processed through a personal computer and plotted by a laser printer. Spectra measured with the Model 2032 analyzer were supplied to a Hewlett-Packard plotter and traced to obtain a hard copy.

TEST RESULTS

ELECTRICAL CHARACTERISTICS

The water table facility was drained and filled with fresh tap water having a specific gravity of 1.000. Salts (in the form of the commercial product named "Instant Ocean") were then added to the water in several steps. At each step, the specific gravity and the currents at various voltages were measured. Figure 6 summarizes the measured electrical conductivity of the simulated seawater as a function of its specific gravity. At a specific gravity of 1.024, a typical value for seawater, the electrical conductivity was 4.5 S/m, which is also consistent with typical published values for seawater. Moreover, the electrical conductivity of the simulated seawater varied linearly with the specific gravity of the water up to specific gravities corresponding to ocean water.

Various dc voltages were applied across the electrodes, and the currents were measured at the different voltage levels. Some of these data are given in Figs. 7 and 8 (for the open-top and closed channels) in terms of applied electric field (E) and current density (j) in order to generalize the variation of channel geometry. Figure 7 summarizes the variation of electric field and current density for the electrolysis process in the open-top channel with metal oxide coated electrodes. Figure 8 provides similar data for aluminum electrodes used in the closed channel. In this latter case, two sets of current-voltage data are shown. The difference between the two curves illustrates the current loss at a given voltage level when the channel was enclosed and the bubbles formed gas pockets in the corners between the electrodes and the insulating wall. (The trapped H_2 gas reduced the effective electrode surface area and hence the current.) The electrical characteristics of these seawater electrolysis channels are discussed in much more detail in ref. 13.

BUBBLE DYNAMICS

The flow channels were constructed from transparent materials so that the bubble generation and bubble dynamics could be observed. Fig. 2 provides a quantitative picture of the bubble behavior.

With the open-top channel configuration (Fig. 4), the electrodes made up the sidewalls channel. Hydrogen generated at the cathode remained in the sidewall boundary layers as sketched in Fig. 2(a). The H_2 bubbles are convected downstream in the sidewall boundary layers, but they also rise due to their buoyancy. As they reach the water surface, they coalesced into much larger bubbles and either escaped from the free surface into the atmosphere or floated downstream on the surface and along the wall forming a "foam boundary layer." In any event, with a free surface, the bubbles did not appear to move out of the sidewall boundary layers where they were generated except when they reached the free surface. Moreover, they rose to the free surface and expanded into the air so that no submerged bubbles were visible at distances greater than one channel length downstream of the channel exit. Figure 9 is a photograph of bubbles formed in an open-top channel. It illustrates (1) the layer of small bubbles forming on the cathode surface, (2) the foam boundary layer at the free surface and (3) the absence of any bubbles in the free stream.

As the bubbles in the surface foam boundary layer burst and the H_2 escaped into the air, there was a faint but audible airborne noise (i.e. a fizzing sound). Prosperetti et al.[25] found that while bubbles bursting on water surfaces create airborne noise, this sound is not transmitted in the liquid. As a result, this fizzing sound was not an important source of water-borne noises during these experiments. As a matter of fact, data from the submerged hydrophone located some distance away from the bursting bubbles were nearly identical to the noise data taken directly under the surface bubble layer. This to some degree confirms Prosperetti's conclusion.

The bubble dynamics in the enclosed channel with the cathode on the bottom wall (floor) were completely different, as illustrated in Fig. 2c. As the bubbles broke away from the cathode wall, they rose through the cathode boundary layer due to their buoyancy and passed into the free stream. Their velocity as they rise in the free stream flow depends upon their size,[19] but for these tests, this velocity was no greater than a few centimeters per second. As a result, the bubbles dispersed through the flow passage and were convected downstream and out of the powered portion of the channel before they rose to the top wall (ceiling). There was one exception: bubbles produced in the bottom corners of the cathode and sidewalls rose through the sidewall boundary layers. Since boundary layer velocities were lower than the free stream velocity, these bubbles rose to the top of the channel before leaving the channel. They subsequently formed small gas pockets in the top corners between the sidewalls and the anode as shown in Fig. 2c. These gas pockets "blocked" a portion of the anode and slightly reduced the current flow as described in ref. 13 and shown in Fig. 8.

While it was not possible to measure or even observe the distribution of bubbles in the free stream (i.e., the void fraction of gas) in the channel for either configuration, some qualitative observations could be made:

1. In the closed channel, the void fraction increased roughly linearly with increasing distance downstream. The bubbles dispersed uniformly across the

free-stream portion of the flow passage and increased in number vertically with increasing axial distance. At the velocities of these tests, they did not quite fill the channel in the vertical direction at the channel exit.

2. In the open channel, the bubbles were confined to the sidewall boundary layers, and most of them had dispersed into the air such that the void fraction was confined to the sidewall boundary layer regions and approached zero about one channel length downstream of the exit.

NOISE MEASUREMENTS AND ANALYSIS

Noise spectra were obtained at frequencies up to 50 kHz for a number of fluid flow and electrical conditions. Figure 10 is characteristic of the noise spectra measured with a voltage applied across the electrodes. Spectra such as these were analyzed over intervals of two decades of frequency to attempt to identify specific sources of the noise.

Test Facility Noise

Figure 11 summarizes the sound pressure levels from 0 to 1600 Hz with and without applied voltage across the electrode walls and with the hydrophone located 7.6 cm downstream of the channel. As a voltage was applied across the electrodes and bubbles formed through electrolysis, the noise spectrum in this frequency range did not change (compare Figs. 11a, 11b and 11c). Also, when the hydrophone was moved several channel lengths downstream, there were only minor changes in the spectrum. In this range, the predominant noise occurred at frequencies between about 30 and 400 or 500 Hz. An accelerometer placed on the water table body and pump also indicated vibrations at these same frequencies. As a result it would appear that sound pressures up to 500 Hz were due to the test facility (i.e., vibrations of the water circulating pump and other parts of the facility). Moreover, noise at these lower frequencies did not change as the bubbles were formed through electrolysis.

Flow Noise

Noise spectra in the frequency range from 200 to 20,000 Hz were also measured when the electrodes were not powered (i.e., $V=0$, $I=0$) at flow velocities from 0 to 70 cm/sec. Two of these spectra are given in Fig. 12 and illustrate additional noise peaks which are associated with the flow. When the circulating pump was shut off and the velocity decreased to zero, all of these peaks disappeared except the peak near 750 Hz. At zero flow velocity, however, water still trickled over the downstream edge of the water table into the exit reservoir. This trickling water was the source of the noise at frequencies near 750 Hz.

Table 1 summarizes particular frequencies (with no applied voltage) which were consistently observed with flow through the channel at different velocities. At zero velocity, the only peak observed was at 736 Hz, which was the peak due to water falling into the exit reservoir. As the flow velocity was increased, additional frequencies began to appear at 1000 Hz and above. These peaks shifted to higher frequencies as the flow velocity increased. At a flow velocity of 70 cm/sec, a harmonic of a 1300 Hz peak at about 2600 Hz was also observed.

Table 1. Measured flow noise frequencies with a closed channel.*

Velocity (cm/sec)	Frequency (Hz)			
0	736	—	—	—
26	768	1024	—	—
50	768	—	1248	—
70	—	—	1306	2592

*The bandwidth at which the frequency spectra were measured was 32 Hz.

Thus, the flow-induced noises in the facility and channel were generally confined to a single predominant peak of 1000 to 1300 Hz, depending on the flow velocity. Moreover, there was no evidence of flow noise at frequencies above 2600 Hz for the velocities of these tests when there was no applied voltage.

Power Supply Noise

A few spectra were obtained using a 12 volt battery powering the electrodes in order to determine if during electrolysis the alternating to direct current power supply was in some way introducing the increased noise levels shown in Fig. 10. As illustrated in Fig. 13, the noise level increased at roughly the same frequencies when the battery supply was used. As a result, it appears that the power supply was not a source of the increased noise that occurred when voltage was applied across the electrodes.

Conditions for Standing Waves

When acoustic reflecting surfaces exist in the vicinity of a noise source, standing waves can exist. In a rectangular enclosure such as these flow channels, standing waves will occur and establish resonant frequencies which depend upon the size of the channel. Because standing waves may form from reflection of acoustic waves normal as well as oblique to the surface, they can be quite complex and give rise to several resonant frequencies. In the simplest case, the sound reflects back and forth between two parallel walls, producing a resonant frequency, f_n, which depends upon the spacing between the walls, or

$$f_n = \frac{nC}{2l} , \tag{11}$$

where C is the speed of sound in the fluid, l is the wall spacing, and n is an integer, since harmonics of the principal wave may also exist.

Calculation of resonant frequencies of standing waves in a bubbly liquid is complicated by the fact that the void fraction of the gas bubbles significantly decreases the effective speed of sound or wave speed in the fluid. Moreover, the decrease depends upon the distribution of bubbles or void fraction in the liquid. The effective wave speed (C_e) in a liquid containing a uniform distribution of gas bubbles at lower frequencies is given by

$$C_e^2 = \frac{C^2}{1 + \beta \varrho C^2 / p_0} , \tag{12}$$

10

where β is the void fraction of the gas, and C is the speed of sound of the liquid with $\beta = 0$. Also, ρ is the fluid density and p_0 is the equilibrium pressure of the bubble in the liquid.

With the enclosed channel, the bubbles are introduced uniformly over the cathode bottom wall and rise through the liquid. Near the exit of the channel and in the exit diffuser the bubbles may be distributed throughout the fluid. In this case, the void fraction, β, may be estimated from the current or current density (Eq. 7); and assuming uniform distribution of β, the speed at which acoustic waves will propagate in bubbly fluid can be determined from Eq. 12. Calculations of wave propagation speeds under these assumptions are summarized in Table 2 for several typical test conditions. With these acoustic wave propagation velocities, the resonant frequencies of standing waves were calculated from Eq. 11 for the dimensions of the enclosed channel. Table 3 lists the effective standing wave frequencies corresponding to various test conditions for the enclosed channel. Since the channel was nearly square (3.4 cm × 3.7 cm), the two standing waves that would exist would probably appear at one frequency corresponding to the mean transverse dimension (i.e., $\approx$ 3.55 cm).

It should be emphasized that in estimating these frequencies, the bubbles were assumed to be distributed uniformly throughout the channel. This condition was only approximately achieved near the channel exit for the conditions of these tests. The effect of void fraction on the calculated values of resonant frequency of standing waves is shown in Fig. 14 together with estimated values of the void fraction for the conditions of these tests.

Standing waves will also exist in the open-top channel. With this configuration, however, two factors alter the resonant frequency of the standing wave. First, the bubbles are not distributed throughout the flow but are confined to the boundary layers. As a result, the gas void fraction should not significantly alter the wave speed from the speed of sound of the liquid. Moreover, since the standing wave frequency is independent of the

Table 2. Wave speeds in a bubbly seawater assuming uniform distribution of the bubbles.

Flow Velocity (cm/sec)	Applied Voltage (V)	Current (A)	Void Fraction	$C_{\bullet}$ (m/sec)
26	8	2.75	0.00119	280
26	15	5.30	0.00230	200
26	24	8.75	0.00380	160
70	8	3.23	0.00047	470
70	15.4	6.36	0.00092	330
70	22.4	10.20	0.00148	240

Table 3. Standing wave frequencies for the enclosed channel .

Flow Velocity (cm/sec)	Applied Voltage (V)	Current (A)	Standing Wave Resonant Frequency (Hz)
26	8	2.75	4000
26	15	5.30	2900
26	24	8.75	2300
70	8	3.23	6170
70	15.4	6.36	4500
70	22.4	10.20	3580

void fraction, it is also independent of the electrical conditions in the channel. Second, the resonant frequency is altered by the existence of a free surface, which serves as a soft reflecting surface opposite from a hard surface. In the horizontal transverse direction with $l = 5$ cm, Eq. 11 suggests that a resonant frequency of 14,750 Hz will exist with the wave speed taken as the speed of sound in salt water, $C = 1475$ m/sec. In the vertical direction Eq. 11 can not be applied because of the "soft" free surface of the fluid. A rough estimate of the standing wave frequency may be made by assuming quarter wave length reflection. This results in a standing wave at 37.5 kHz.

Bubble Noise

Another possible noise source is the oscillation of the bubbles as they adjust to an equilibrium spherical shape. The diameters of oscillating bubbles were calculated from the Minnaert equation (Eq. 9) for the range of frequency covered by these tests;* they are shown in Fig. 15. These calculations were made for a pressure of 1 atm and a specific heat ratio of the gas of 1.4. At these conditions, a 1–mm–diameter bubble will oscillate at about 3000 Hz, while a 0.1–mm–diameter bubble will oscillate at about 40 kHz. The frequency range of noise measured during these tests corresponds to bubble diameters from about 0.1 to 2 mm, which is consistent with visual observation of the bubble size. Unfortunately, no independent measurement of bubble diameter could be made during these tests.

DISCUSSION OF NOISE TEST RESULTS

Bubble noise data were obtained as a secondary activity in investigating the electrical characteristics of a seawater MHD thruster reported in ref. 13. Consequently, noise data were not obtained as systematically as were the electrical measurements reported in ref. 13. While these results should be viewed as preliminary, they may be useful in beginning to understand and assess the noise characteristics of MHD seawater propulsion systems. Although these were small-scale experiments, they still may aid in guiding subsequent testing of large MHD seawater thrusters.

---

* The calculations assumed that the polytropic exponent governing the expansion and contraction of the gas bubble could be approximated by the specific heat ratio. This assumption would result in estimates of bubble size which would be no more than 10% too large.

Noise data were obtained with both the enclosed channel and the open-top channel at various test conditions, as summarized in Table 4.

ENCLOSED CHANNEL

Figures 16, 17 and 18 present the measured noise spectra for the enclosed channel at frequencies up to 25 kHz. Sound pressure levels at higher frequency were essentially constant with no detectable sound pressure level peaks or sound pressure levels above the base level (i.e., a flat spectrum). The measured noise spectrum with no applied voltage or current is also shown on these figures for comparison. With no current flow, the noise spectrum was flat above about 1500 Hz. The increase in noise at lower frequencies was caused by the facility and flow noises, as described previously.

As current began to flow across the channel and electrolysis bubbles were formed, there was a broad-band increase in the noise level downstream of the channel (and upstream; see Fig. 16) at frequencies from roughly 2.5 kHz to about 20 kHz, depending upon the flow velocity. Bubbles generated at the walls appeared visually to be 0.1 to 0.5 mm in diameter. As they moved into the free stream, they coalesced and, as might be expected, they appear to form a broad distribution of bubble sizes. This broad size distribution would explain the observed broad-band noise spectrum. In addition, there were several noise peaks at a few individual frequencies. The cause of these peaks is also of interest.

Zero Flow Velocity

Figure 16 presents two noise spectra taken under static conditions with a current flow of about 5 A and with zero flow velocity. With no flow through the channel and the cathode as the lower wall, the bubbles (and hence the gas void fraction) would be expected to be more or less uniformly distributed in the channel volume, and would satisfy the assumption made in the calculation of the resonant frequency for standing waves. The rise velocity of H_2 bubbles in the channel was estimated to be about 5 cm/sec (consistent with data of Richardson[19]), which leads to a residence time of 0.75 sec for the bubbles in the channel when there is no axial velocity. At a current of 5 A the attendant void fraction was calculated to be 0.0028. With this void fraction, the frequencies of standing waves

Table 4. Summary of test conditions for acoustic data .

Channel	Flow Velocity (m/sec)	Applied Voltage (V)	Current (A)	Figure Number
Enclosed	≈0	15.5	5	16
Enclosed	26	8	2.74	17
	26	15	5.30	17
	26	24	8.75	17
Enclosed	70	8	3.23	18
	70	15.35	6.36	18
	70	22.75	10.20	18
Open	47	30	5.1	19

with zero axial velocity would be multiples of about 2600 Hz. Inspection of Fig. 16a reveals that the most pronounced noise peak occurred at 2784 Hz (highlighted by the box). This peak is most likely associated with a standing wave. There were also much weaker but noticeable noise peaks at about 5000 and 7500 Hz. The source of the peaks is not known, but they are close to harmonics of the principal standing wave frequency. Noise peaks observed at frequencies below 1 kHz were most probably due to the noise of water trickling from the facility as the exit reservoir drained. Thus, with no axial flow, the noise due to bubbles occurred over a frequency range from about 2 to 20 kHz. This would correspond to bubble sizes from about 0.3 to 3 mm in diameter. The superimposed peaks observed in the Fig. 16 data are in all likelihood the result of standing waves.

Flow Velocity of 26 cm/sec

Figure 17 summarizes the bubble noise spectra at a flow velocity of 26 cm/sec. Again, broad-band noise occurred with superimposed noise peaks at specific frequencies. As the current increased, more bubbles were generated, and the noise levels (i.e., sound pressure levels) rose, as would be expected. (Compare Figs. 17a, b, and c.) Analysis of these individual noise peaks is also interesting.

At lower frequencies, peaks were observed at 768 Hz and at 1024 Hz with a velocity of 26 cm/sec. These peaks were due to flow noises, as discussed previously. Some of the other peaks visible in Fig. 17 are also associated with standing waves. Table 5 compares previously calculated standing wave frequencies with the frequency of noises peaks evident in Fig. 17.

The observed frequencies were surprisingly close to the predicted values for standing waves, considering that the predictions assume a uniform distribution of bubbles. A closer inspection of these peaks provides more convincing evidence that they are associated with standing waves.

As shown by Fig. 14, the resonant frequency of a standing wave decreases with increasing void fraction (i.e., increasing current). This effect can be seen both in Figs. 17 and 18. At an applied voltage of 8 V and current of 2.75 A, the peak believed to be a standing wave is at 3968 Hz (Fig. 17a). Another noise peak is near 3400 Hz. As the current was increased to 5.3 A, the standing wave frequency decreased to about 3000 Hz (See Fig. 14). As a result, the standing wave peak merged with the noise peak at about 3400 Hz, producing the stronger and broader peak observed in Fig. 17b, which was centered at 3040 Hz. As the current was further increased to 8.75 A (Fig. 17c), the standing wave frequency shifted further to the left (to lower frequency) and to a frequency of 2528 Hz, which again exposed the peak that remained near 3400 Hz. These three noise spectra

Table 5. Comparison of calculated standing wave resonant frequencies with frequencies of noise peaks observed in Fig. 17; Velocity = 26 cm/sec .

Voltage (V)	Current (A)	Calculated Frequency of Standing Wave (Hz)	Figure 17 Frequencies (Hz)
8	2.75	4100	3968
15	5.30	3000	3040
24	8.75	2400	2528

show, in effect, the standing wave peak shifting to lower frequency with increasing current. As was the case with zero flow velocity, the most dominant bubble noise peaks at this velocity appeared to be associated with a standing wave.

At a velocity of 26 cm/sec, the bubbles produced broad-band noise between about 2500 and 13,000 Hz. In addition, there were specific noise peaks at frequencies near 3400, 5000 and 8200 Hz at all levels of current. Since these peaks did not shift with increasing current, they do not appear to be harmonics of the standing wave.

Flow Velocity of 70 cm/sec

Figure 18 provides the noise spectra at three current levels when the flow velocity was 70 cm/sec. Table 6 compares the calculated standing wave frequencies with the frequencies of some peaks observed in Fig. 18.

Closer inspection of Fig. 18 again reveals at least a partial picture of some peaks shifting to lower frequencies with increasing current. At a current of 3.23 A, the noise peak at 6048 Hz shown in Fig. 18a is close to the calculated standing wave resonance frequency of 6170 Hz. Figure 18a also indicates a noise peak at 4288 Hz. As the current increased to 6.36 A (Fig. 19b), the frequency for a standing wave would decrease to about 4500 Hz. Consequently, one would expect a strong and broad peak at about 4400 Hz. The Fig. 18b spectrum doesn't exhibit a peak in this range. Moreover, it does not show the 4288 Hz peak that was evident at the lower current flow. However, when the current was increased further to 10.20 A, a new peak appeared at 3584 Hz, which is close to the calculated value for a standing wave. In addition, the peak at 4288 Hz reappeared. Thus, these data suggest the existence of a standing wave which shifts to lower frequency with increasing current. The anomaly of a "disappearing peak" near 4300 kHz in Fig. 18b is unexplained.

At a flow velocity of 70 cm/sec, increasing the current increased the bubble noise level (Compare Figs. 18a, 18b, and 18c). Also, at this higher velocity, the noise was confined to lower frequencies between about 2000 and 9000 Hz. In addition, there appeared to be stronger superimposed noise peaks at about 2600 Hz and 4300 Hz.

Effect of Flow Velocity

The effect of flow velocity on the noise spectra is summarized by Fig. 20, which compares the measured spectra at three velocities with the same applied voltage. Increasing the velocity decreased the maximum frequency over which bubble noise occurred from about 19 kHz at zero velocity to 9 kHz at a velocity of 70 cm/sec. This suggests that

Table 6. Comparison of calculated standing wave resonant frequency with frequencies of noise peaks observed in Fig. 18; velocity = 70 cm/sec.

Voltage (V)	Current (A)	Calculated Frequency of Standing Wave (Hz)	Figure 18 Frequency (Hz)
8.01	3.23	6170	6048
15.35	6.36	4500	—
22.75	10.20	3580	3584

while the residence time for bubble coalesce decreases with increasing velocity, the higher velocities may result in a greater degree of coalesce of the bubbles, which would shift the bubbles size distribution to larger diameter bubbles.

Excluding the noise peaks associated with the flow and those believed to result from standing waves, a few other frequencies exhibited noise levels above the broad-band noise introduced by the bubbles. The frequencies of these superimposed noise peaks as shown in Fig. 20 and given in Table 7.

In general, these frequencies tended to decrease with increasing flow velocities, which also suggests that larger bubbles exist in the higher velocity flows. If these superimposed peaks are specific to a particular bubble size, the bubble diameter could be estimated from Fig. 15.

Table 7. Summary of sound pressure level of superimposed peaks in Fig. 20.

	Flow Velocity		
	0	26 cm/sec	70 cm/sec
Frequency of	4220	3400	2560
Specific Peaks	4960	5216	2980
	7600	8160	5760

OPEN-TOP CHANNEL

Figure 19 presents some noise spectra for the open-top channel configuration with a velocity of 47 cm/sec and a current of about 5.5 A. Most of the testing carried out for this channel configuration was to evaluate long-duration electrode performance. Consequently, the test conditions were held constant; the bubble noise data thus correspond to a single electrical test condition. As noted earlier, these noise spectra are complicated by the "soft" reflecting surface represented by the free surface of the water, and this configuration is not representative of a seawater MHD thruster. However, there are several interesting features of these spectra.

First, the overall sound pressure levels with the open-top configuration were roughly two orders of magnitude lower than those measured in the enclosed channels. As described previously, the bubbles were confined to the sidewall boundary layers in this channel, and the void fraction over the bulk of the channel volume was essentially zero. Moreover, the bubbles rose to the surface in the boundary layers and escaped into the ambient air. No bubbles could be observed in the flow beyond a few centimeters down stream of the channel exit. With less opportunity for bubbles to coalesce, the noise level was greatly reduced.*

---

*In addition, the author is indebted to Theodore Farabee (DTRC) for pointing out that "this combination of a soft and hard boundary results in a wave-guide which is characterized by its cut-off frequency. Below the cut-off frequency, propagation does not occur but instead the acoustic field is evanescent and decays exponentially." For the conditions of these tests, the cut-off frequency would be about 18 kHz. This factor also contributes to lower noise levels with the open-top channel and may be responsible for the absence of sound pressure level peaks a frequencies below 15 to 18 kHz observed in Fig. 19.

Inspection of the noise spectra (Fig. 19a) again reveals broad-band noise, a broad and prominent peak centered at about 34 kHz. Also, there is a secondary peak at 11 kHz. This latter peak is in the frequency range of the calculated standing wave between the two electrode walls (approx. 14,750 Hz).

The sound pressure level peak at 34 kHz is interesting. If it is associated with bubble oscillations, the bubbles would be about 0.1 mm in diameter. A reasonable speculation is that this is bubble noise which is associated with bubbles breaking away and detaching from the wall. If that is the case, the frequency of the noise indicates which the bubbles that break away are nominally between 0.075 and 0.12 mm in diameter (see Fig. 15). It might also be noted that the peak centered at 34 kHz is close to a frequency of a standing wave corresponding to a quarter wavelength wave between the bottom hard surface and water's free surface, which would have a frequency around 37.5 kHz. No peaks were evident in this spectrum at frequencies below 11 kHz (see footnote on page 16).

The noise spectrum shown in Fig. 19b was measured 2 hours after that of Fig. 19a. It exhibits noise peaks at three lower frequencies, which were not present at the start of the test (Fig. 19a). Over the 2-hour test period, the temperature of the seawater electrolyte increased several degrees. As a result, the additional noise peaks at frequencies of 2.1, 2.9 and 5.2 kHz may be due to additional bubble formation as O_2 outgasses from the heated water. At a later time in this continuous test, these three noise peaks again disappeared. If this speculation is correct, then it will be difficult to accurately assess bubble noise in closed recirculating test facilities unless the water temperature is maintained at a relatively constant value.

BUBBLE SIZE

Since the frequency at which bubbles oscillate depends upon their size (Eqs. 9 and 10), the noise spectra can be used to make a passive estimate of the bubble diameter. The broad-band noise produced in the closed channel when electrolysis was begun (as indicated by Fig. 15) would suggest bubble diameters from about 1 mm to perhaps as low as 0.15 mm. This size range is larger than some results reported by Janssen and Hoogland[26] for electrolytically produced H_2 and O_2 bubbles at detachment. Noise spectra from the enclosed channel tests indicate bubble diameters perhaps an order of magnitude larger than the ref. 26 data. It might be noted that the noise peak centered around 34 kHz, which was observed with the open-top channel, corresponds to a bubble size ($d < 0.1$ mm) much closer than Janssen and Hoogland data. It was noted earlier that this peak is believed to be associated with the detachment of bubbles from the electrodes since with this configuration, the bubbles did not move into the free stream and did not have the opportunity to coalesce with other bubbles. They were observed to just stream up to the free surface through the sidewall electrode boundary layer. One possible conclusion from these comparisons is that the enclosed channel having the cathode surface on the floor allows the bubbles to quickly pass into the free stream and gives them a much greater opportunity for bubbles to coalesce and form larger bubbles which oscillate at lower frequencies. As a result, the bubble noise spectra shown in Figs. 16, 17 and 18 may be dominated by noise associated with bubble coalescence, rather than detachment of bubbles from the wall.

Data presented by Blouchard and Woodcock[21] illustrates that lower frequency bubble noise will not be attenuated as much as high frequency noise.

STANDING WAVES

The bubble noise spectra measured with these small channels consistently indicate the existence of standing waves. Furthermore, the resonant frequencies of these waves is in the same frequency range as the oscillating bubble noise. This makes interpreting and understanding electrolysis bubble noise difficult in small-scale tests such as this one.

In larger seawater MHD thrusters and at the scale of submerged vessels, the frequency of standing waves would be quite low. For example, a $1 \times 1 \times 6$ meter long channel with a flow velocity of 10 m/sec and a current density of 0.3 A/cm^2 would have standing wave frequencies much lower than those produced by flow turbulence (i.e., below 250 Hz). Furthermore, depending upon the spatial distribution of the bubbles, standing wave resonant frequencies could be less than 50 Hz. Thus, bubble noise analysis and interpretation should be much simpler in large channels.

CONCLUDING REMARKS

Sound pressure levels were measured as a function of frequency in a small-scale MHD-type channel (without an applied magnetic field) using a hydrophone which protruded into the flow. These tests were carried out during electrolysis of salt water and at flow velocities of 0 to 70 cm/sec. The current densities ranged up to 0.3 A/cm^2. These tests provide preliminary measurements of the H$_2$ bubble noise that will occur in an MHD seawater thruster. While the scale and flow velocities for the tests were low compared to projected seawater MHD thrusters, the measurements are of interest and may aid in the testing and evaluation of larger seawater thrusters. Some conclusions have been drawn from these data.

1. The production of hydrogen bubbles through the electrolysis of seawater at current densities expected for MHD ship propulsion, 0.1 to 0.3 A/cm^2, produced a broad-band increase in the sound pressure level at frequencies from about 2 to nearly 20 kHz. The upper range of this frequency interval decreased with increasing flow velocity. The incremental increase in the sound pressure level or noise due to the electrolysis bubbles roughly doubled from 0.015 pascals without current flow to about 0.030 pascals at current densities between about 0.2 and 0.3 A/cm^2. The noise level of the bubbles increased with increasing current over the range of currents covered in this investigation.

2. A few noise peaks at specific frequencies were superimposed on the broad-band noise. The most significant of these, however, appeared to be associated with standing waves that existed in these small scale channels. When the H$_2$ bubbles were introduced by the cathode at the floor of the channel, they rose through the boundary layer due to their buoyancy and were dispersed in the free stream, giving rise to an increasing void fraction in the free stream with increasing downstream distance. The void fraction increased with increasing current; a small change in void fraction significantly affects the wave speed and hence the frequencies of standing waves. Standing wave resonant frequencies for the conditions of these tests varied between about 2.5 and 6 kHz in the enclosed channel configurations and depended upon the current, flow velocity and size of the channel. These standing waves complicate the interpretation of the acoustic data. A larger scale MHD seawater thruster, in contrast, will not produce standing waves at frequencies this high and in the bubble noise range.
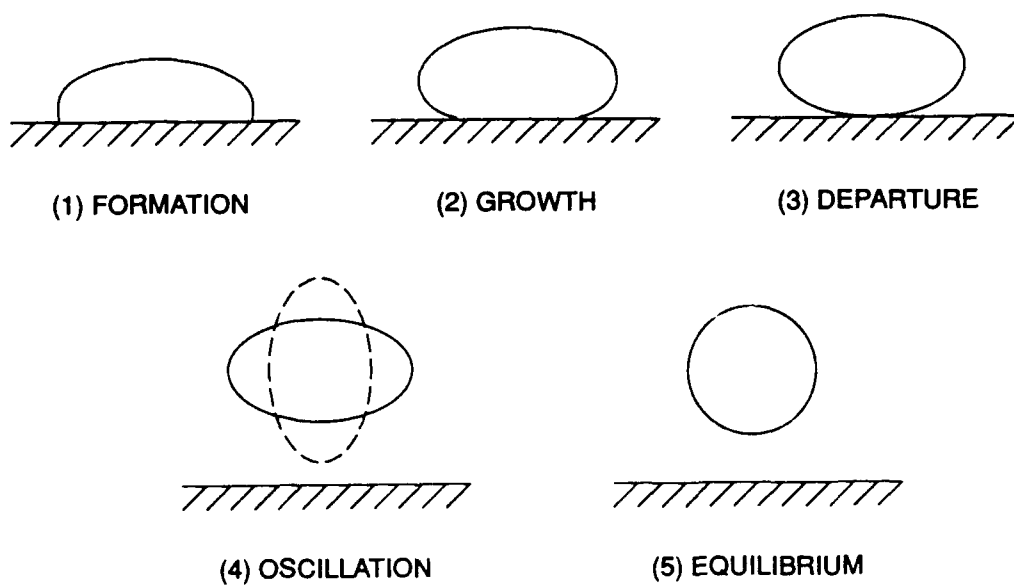
3. In total, these acoustic data suggest that bubble oscillation following the coalescence of bubbles in the free stream may be the principal noise source with an enclosed channel. Bubbles which detach from the wall also produce noise, but at sound pressure levels which are only a few percent of the levels produced by coalescing bubbles. This division of noise is to some degree conjectural.

4. The broad-band noise in a closed channel would suggest through Minnaert's equation[17] that the coalescing H_2 bubbles ranged from about 0.15 to more than 1 mm in diameter. Other test results in an open-top channel, in which the bubbles only resided in the sidewall boundary layers and rose vertically to escape in the ambient air, appeared to produce a sound pressure peak centered about 34 kHz. This noise peak is believed to be associated with bubbles detaching from the electrode surfaces and corresponds to bubble diameters of 0.075 to 0.15 mm for detaching bubbles. This size range inferred from the noise spectra is somewhat higher than other photographic measurements reported by others.

5. The frequencies of bubble noise measured in these tests are consistent with some results obtain in Germany in the 1950's. Noise from H_2 bubbles at frequencies above 20 kHz should be highly attenuated. Thus, bubble noise which appears to be associated with detachment from the electrodes may not be significant in MHD thrusters. However, noise produced by coalescing bubbles occurs at much lower frequency, perhaps under 5 kHz, and it may not be significantly attenuated by the water.

6. The possibility of biological films coating the bubbles in real ocean water was not considered in these tests. Such films could greatly alter the acoustics of electrolysis bubbles. While this phenomenon may be important only near surface ocean waters, it should be investigated, nevertheless, because of the large effect it could have on amplitude and frequency of bubble noise.
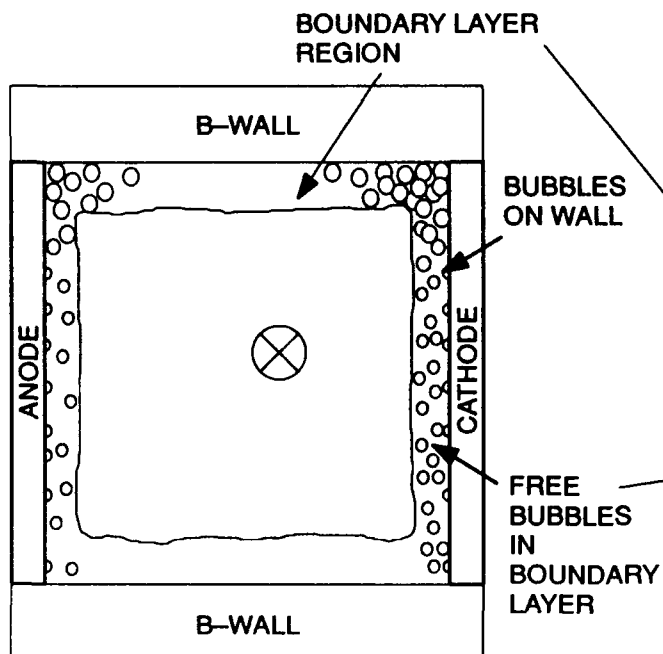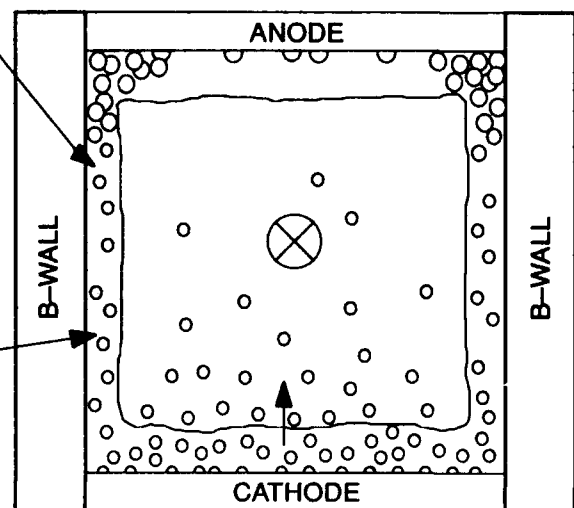
FIGURES

(1) FORMATION   **(2) GROWTH**   **(3) DEPARTURE**

(4) OSCILLATION   **(5) EQUILIBRIUM**

(a) Electrolysis bubble dynamics.

(1) CONTACT   **(2) COHESION**

(3) OSCILLATION   **(4) EQUILIBRIUM**

(b)

Fig. 1. Bubble oscillation.

FOAM BOUNDARY LAYER
ON FREE SURFACE

FREE SURFACE

ANODE

CATHODE

FEWER
BUBBLES

NO BUBBLES
IN THE
FREE STREAM

BUBBLE ON WALL

FREE BUBBLES
RISE VERTICALLY

BOTTOM WALL (FLOOR)
BOUNDARY LAYER REGION –
NO BUBBLES

(a)   Open top channel.

⊗ FLOW INTO
THE PAGE

BOUNDARY LAYER
REGION

B–WALL

ANODE

CATHODE

⊗

B–WALL

BUBBLES
ON WALL

FREE
BUBBLES
IN
BOUNDARY
LAYER

ANODE

B–WALL

B–WALL

⊗

CATHODE
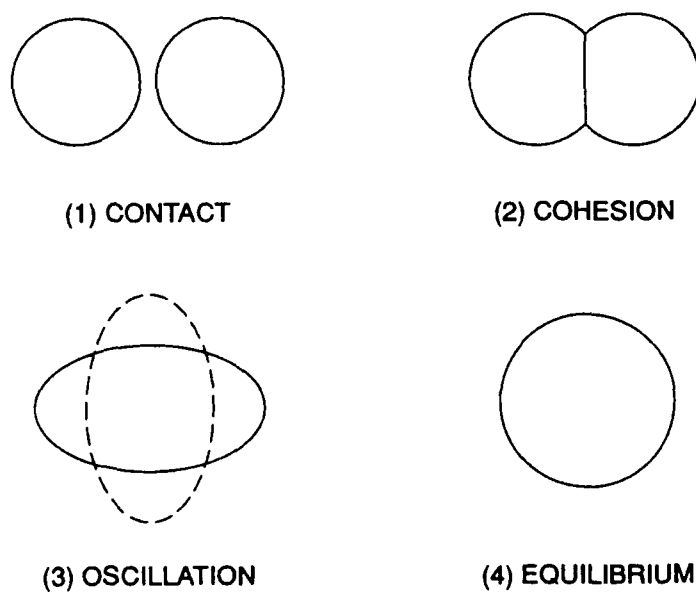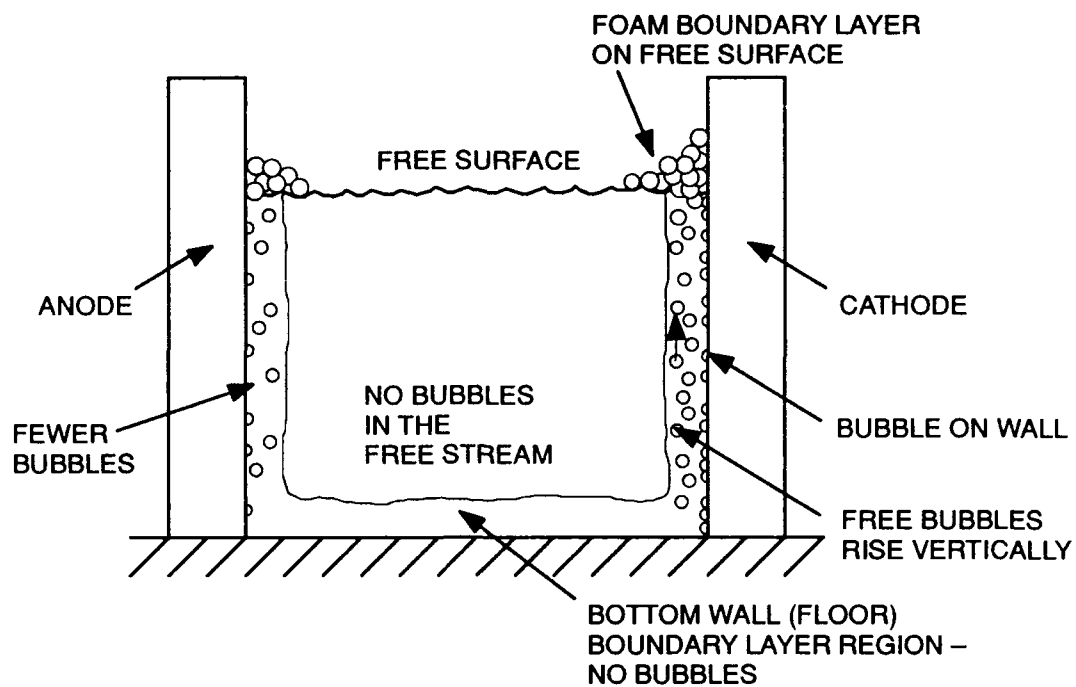
(b)   Closed channel:
       electrodes on the
       sidewalls.

(c)   Closed channel:
       electrodes on top
       & bottom.

Fig. 2.   Bubble dynamics in the electrolysis process in open and closed channels.
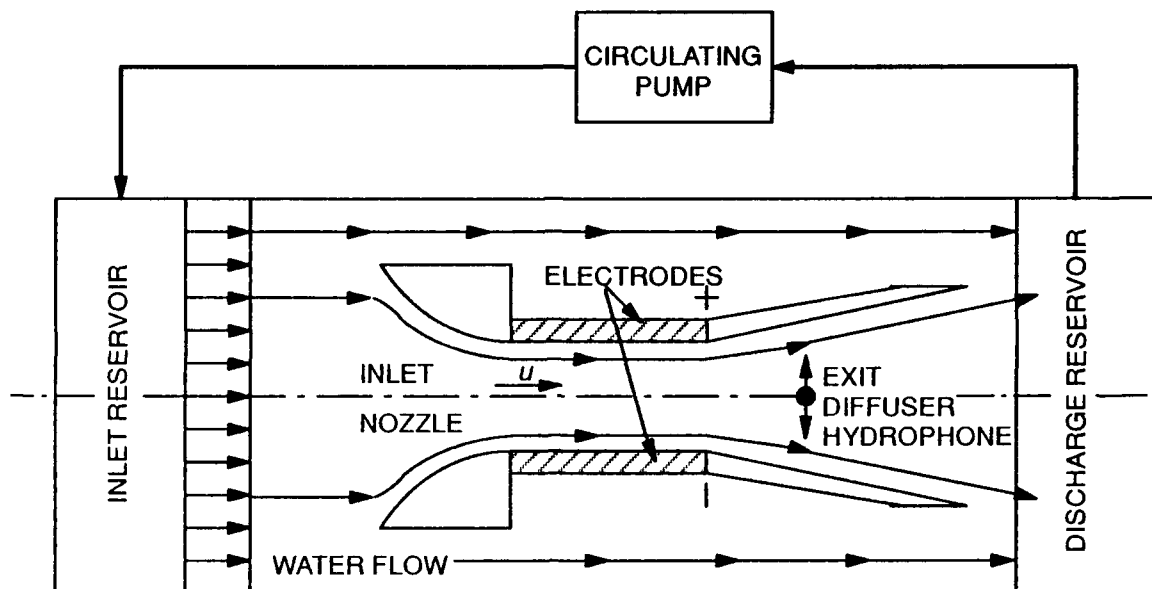
Fig. 3. Schematic of the test set-up for the open-top channel tests.
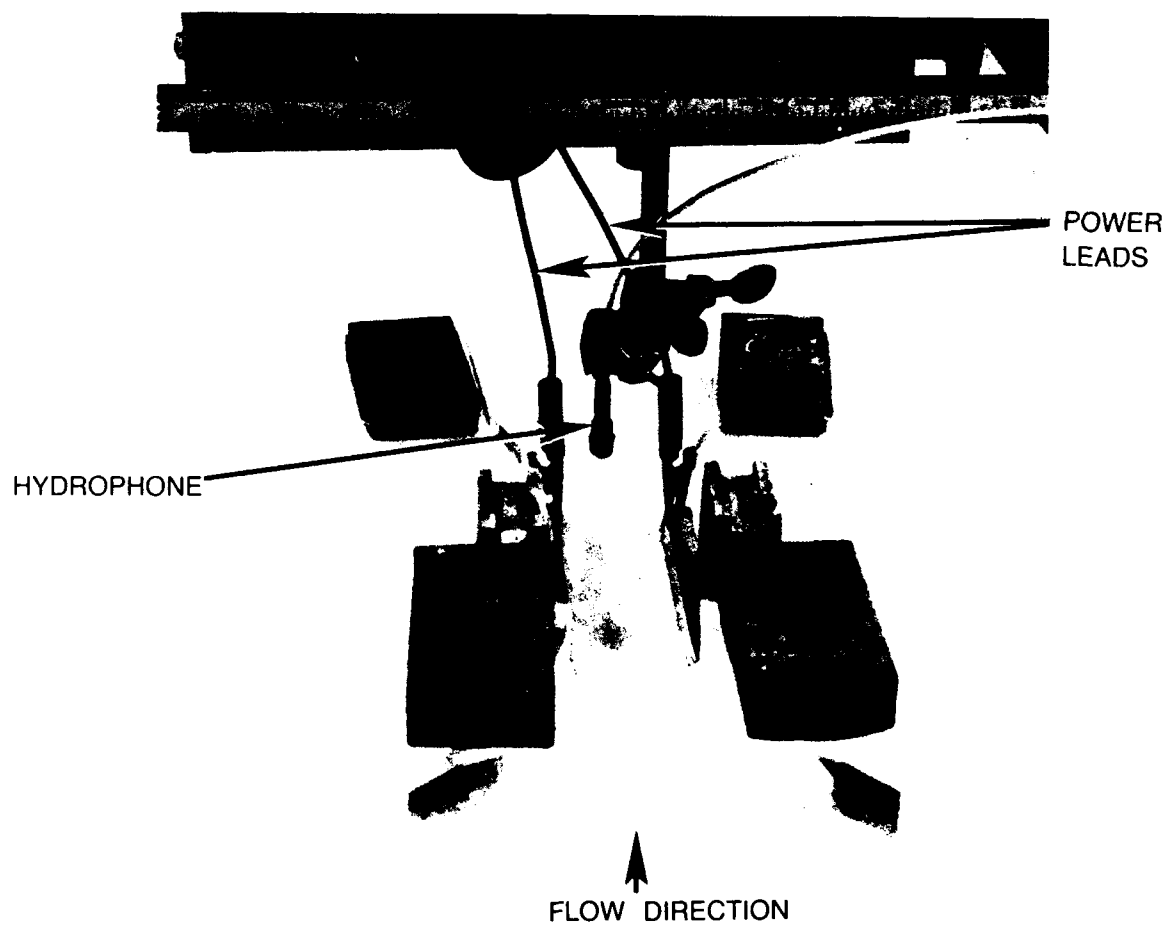
Fig. 4. Photograph of the open-top channel configuration.
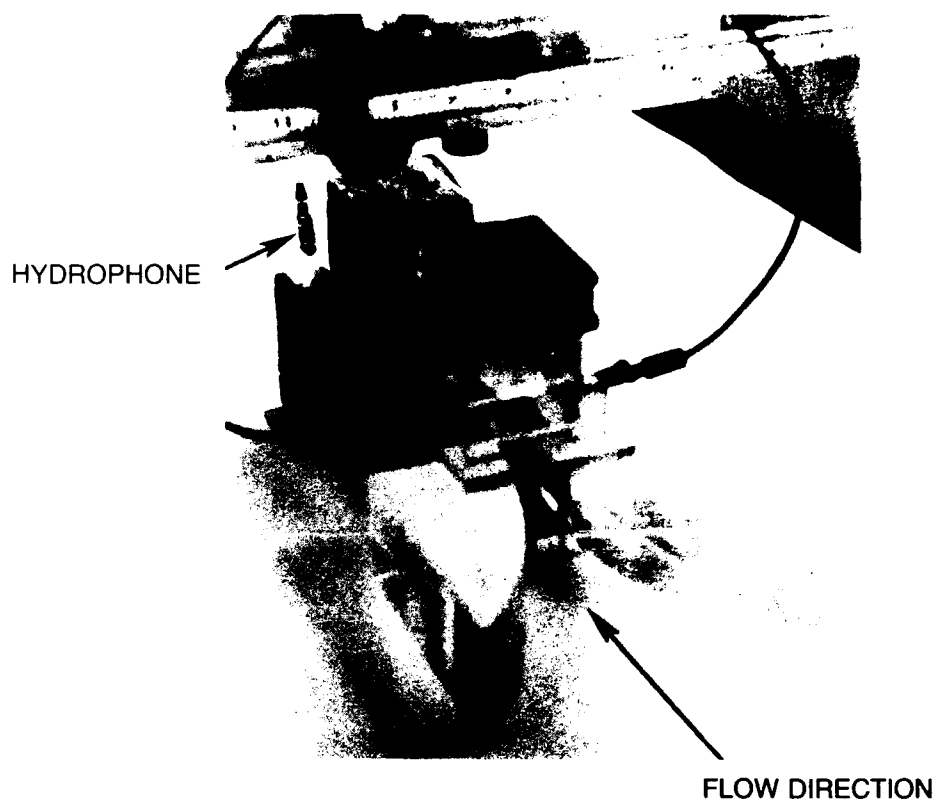
Fig. 5. Photograph of the closed channel configuration.
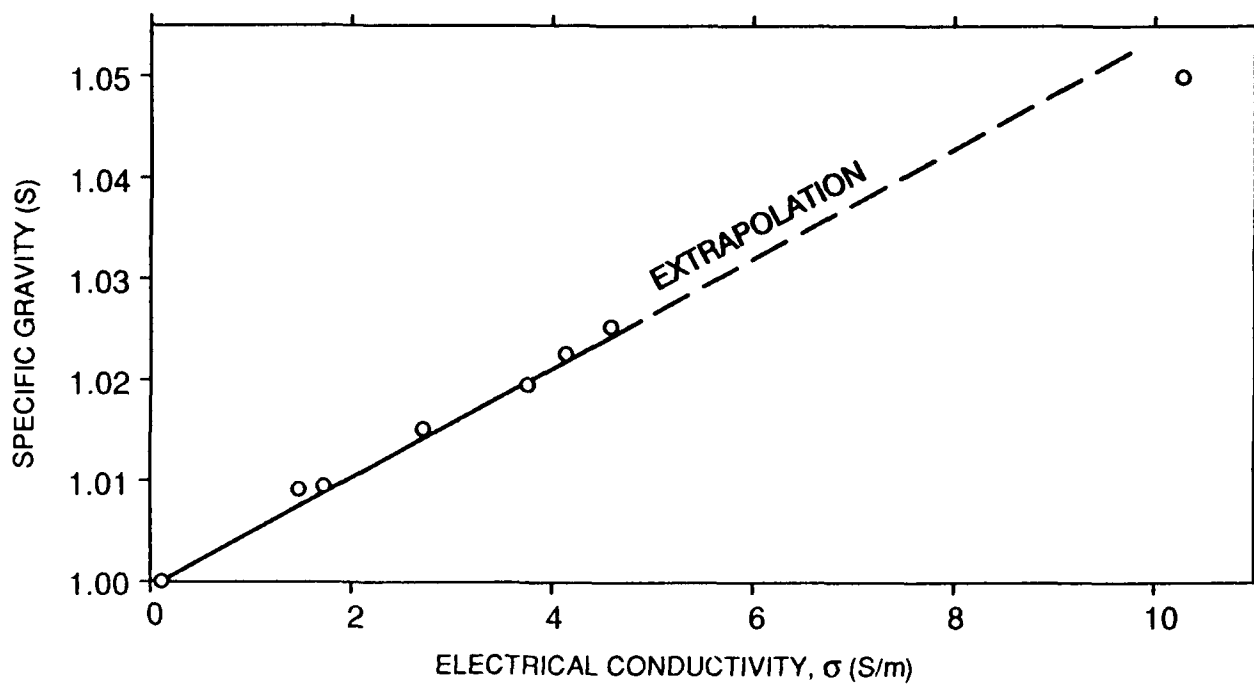
Fig. 6. Variation of measured electrical conductivity with specific gravity for simulated sea water.
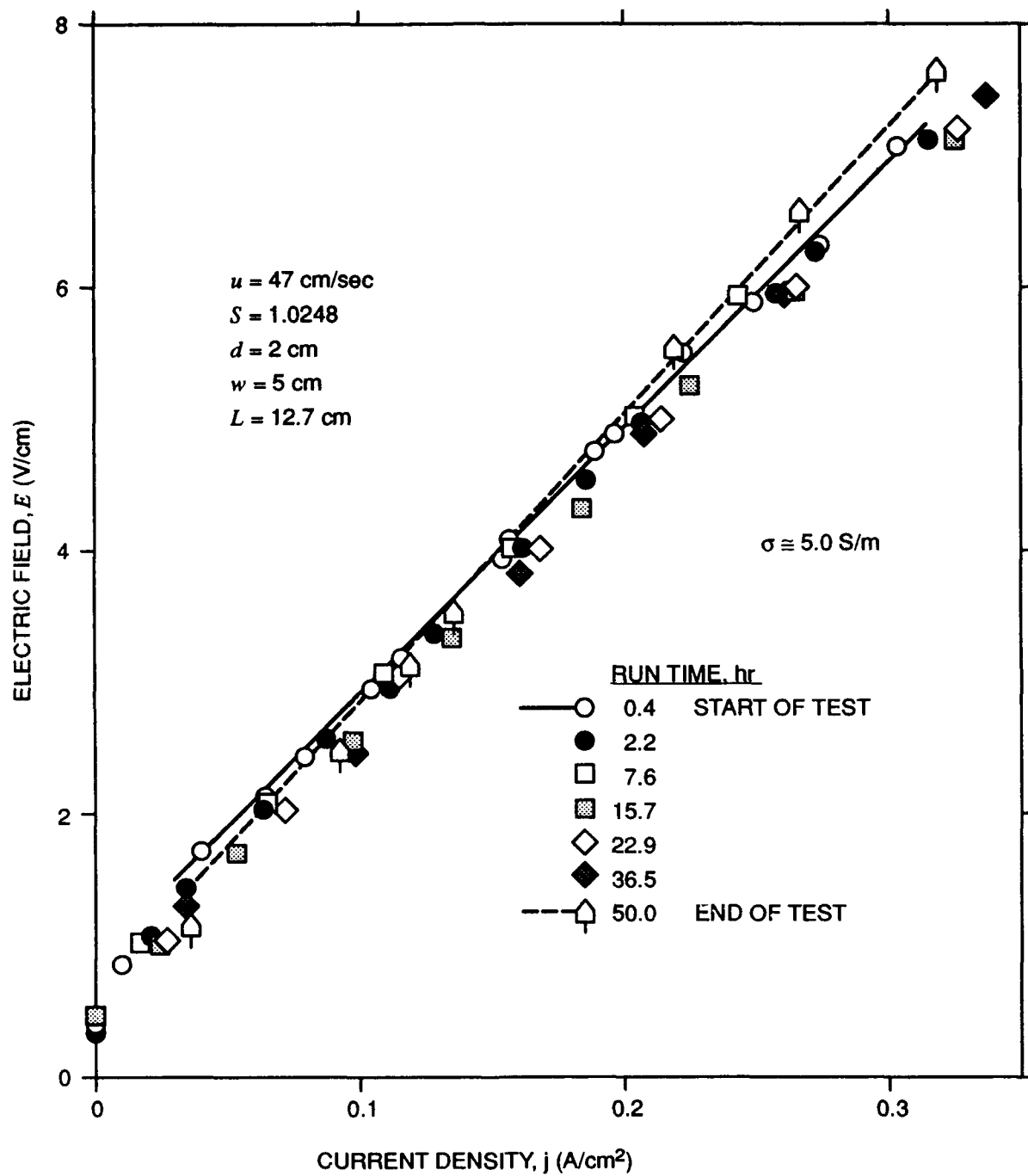
Fig. 7. Current density variation with electric field for Eltech electrodes.
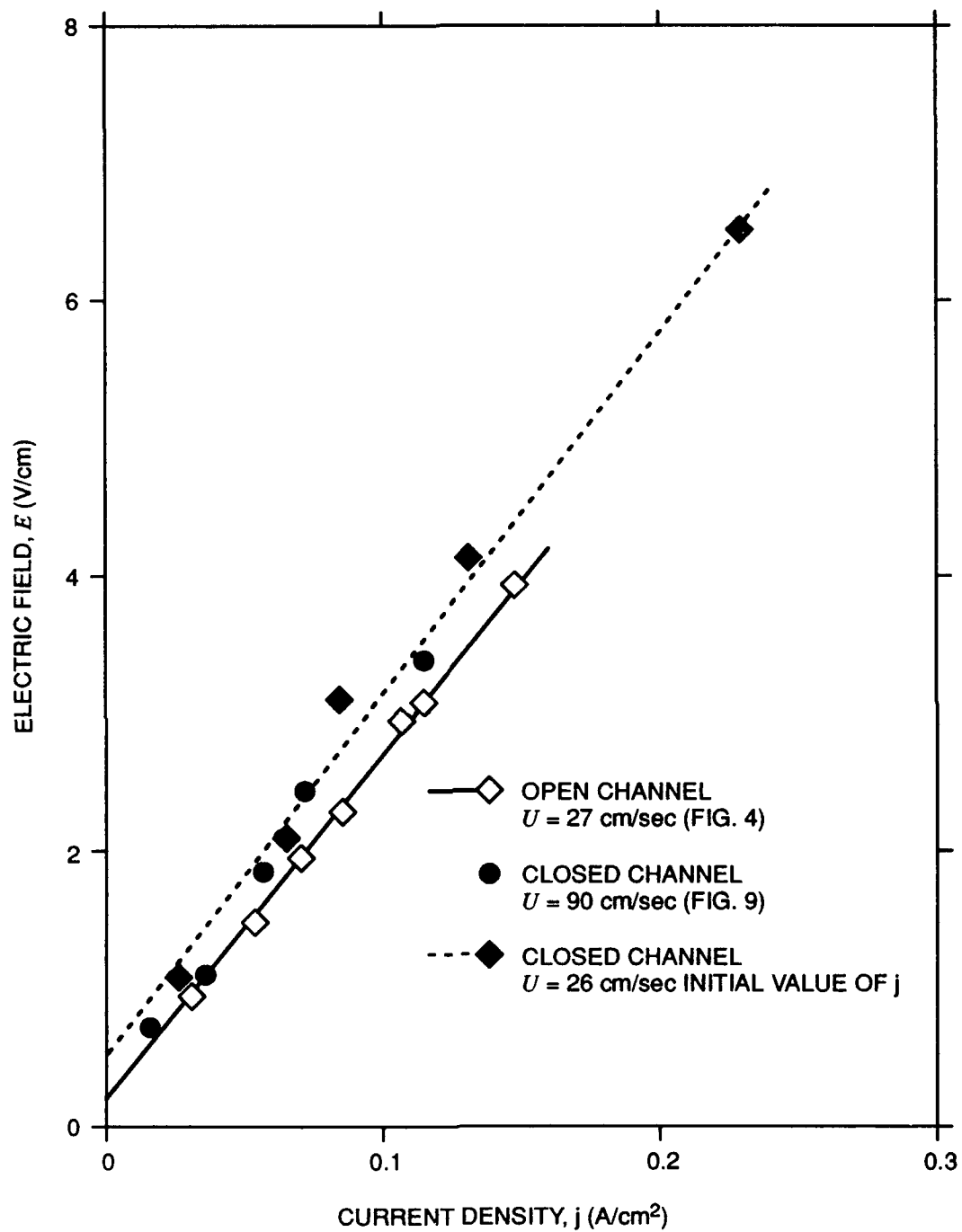
Fig. 8. Current density variation with electric field for an enclosed channel at various run conditions.

Fig. 9. Photograph of bubbles formed in the open-top channel.
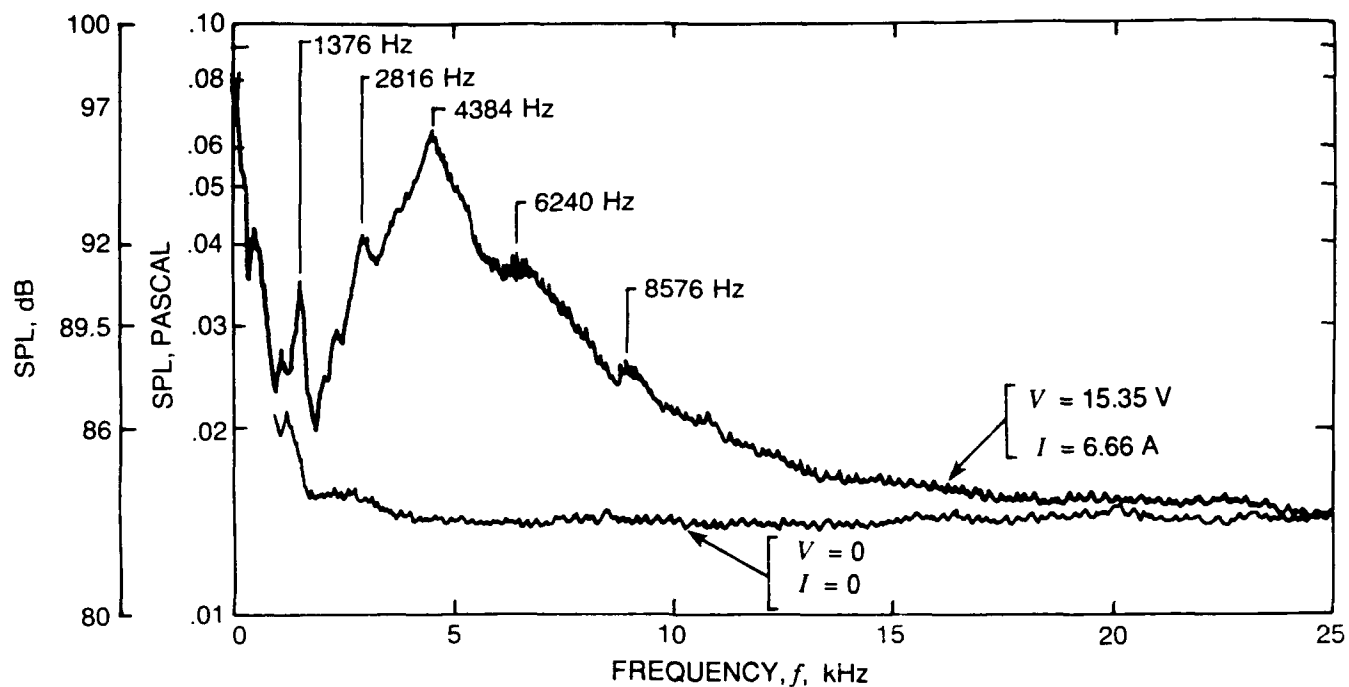
(a) Hydrophone 5-cm upstream, V = 15.35 volts.
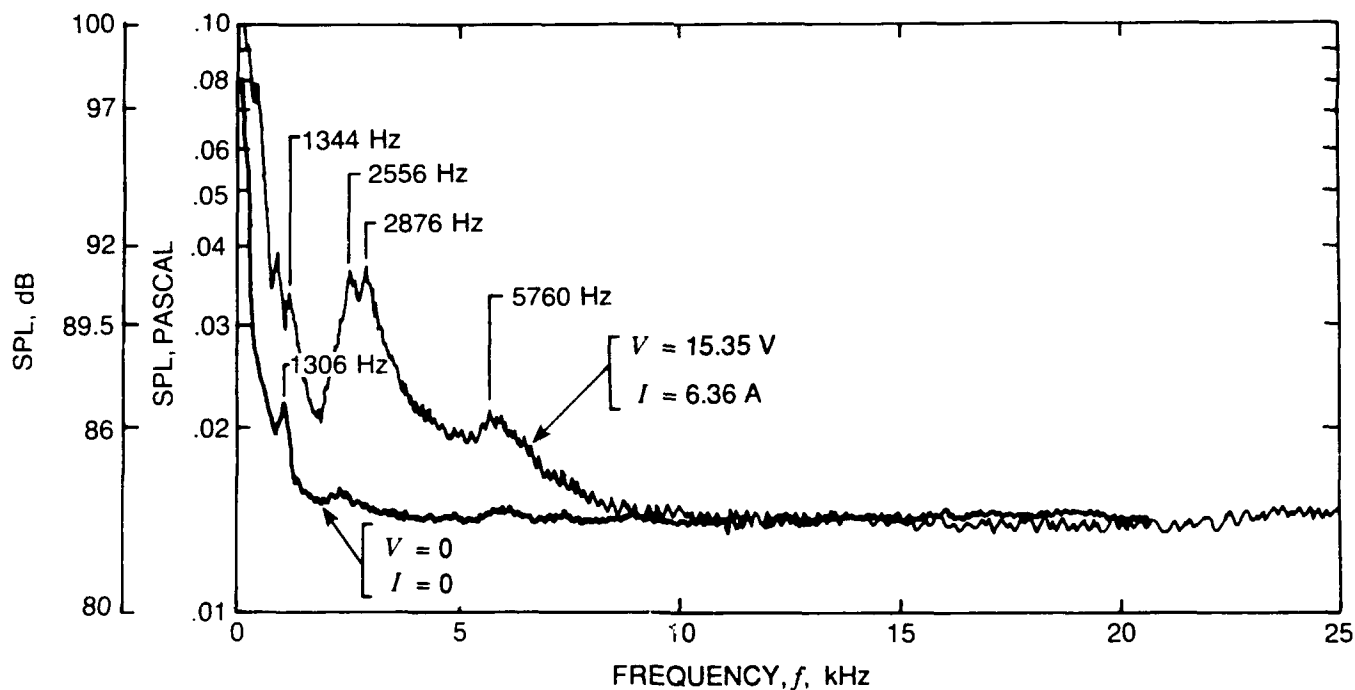
(b) Hydrophone 10-cm downstream, V = 15.35 volts.

Fig. 10. Enclosed channel noise spectra; flow velocity = 70 cm/sec.
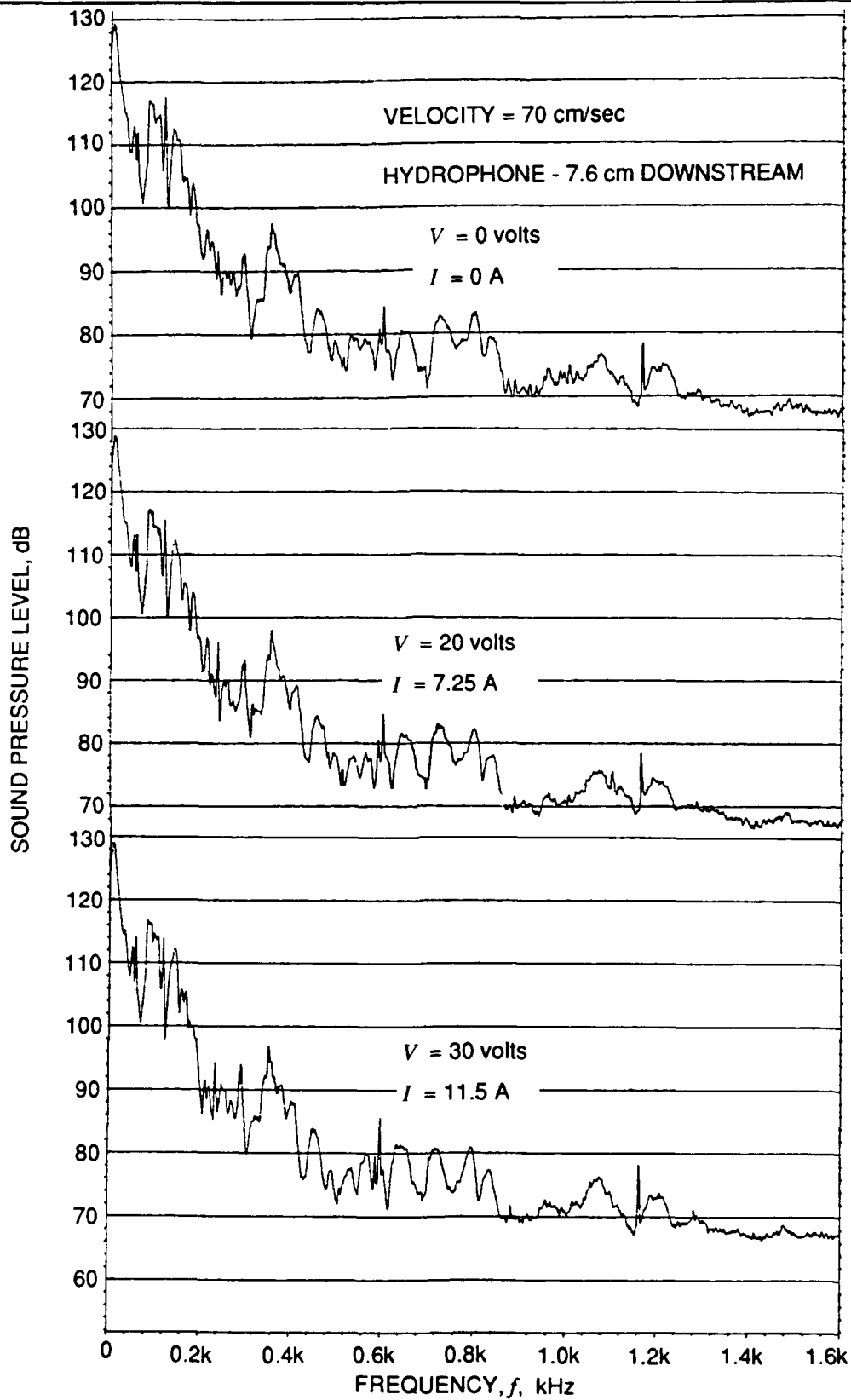
Fig. 11. Low frequency noise spectra.
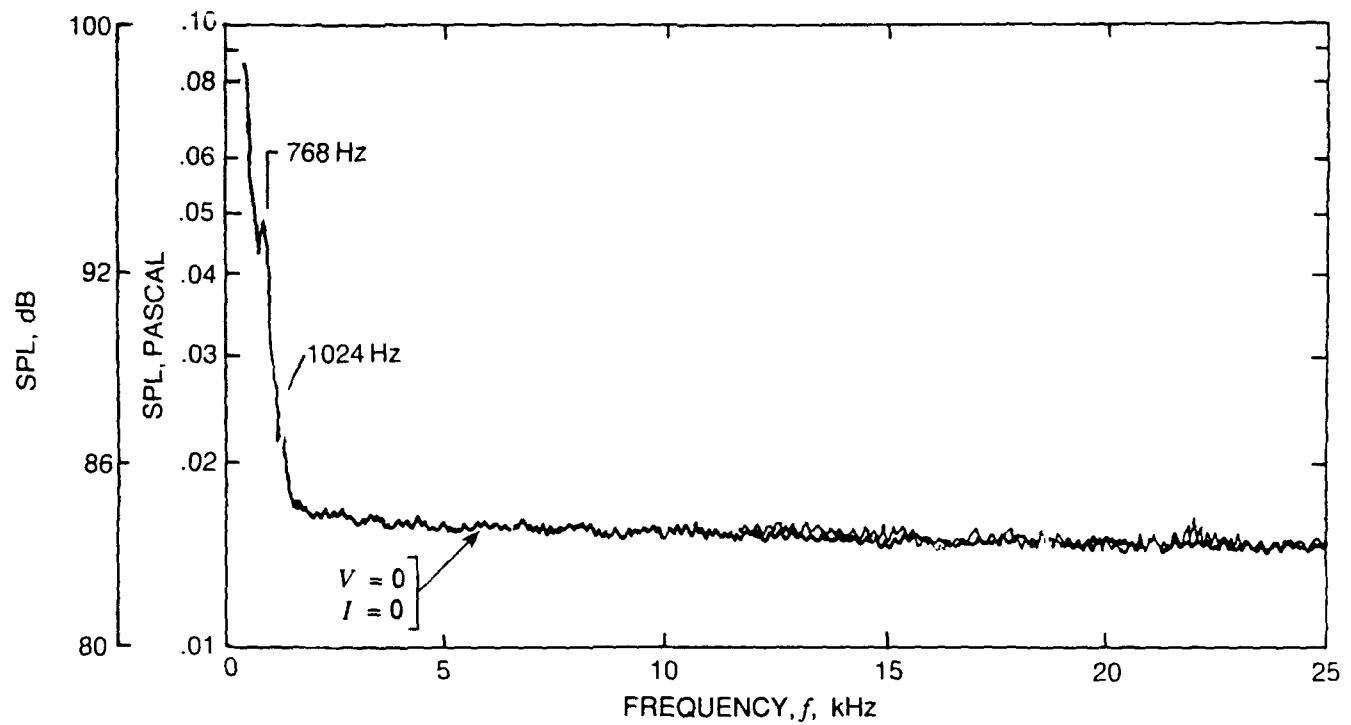
(a) Enclosed channel noise spectra, flow velocity 26 cm/sec.
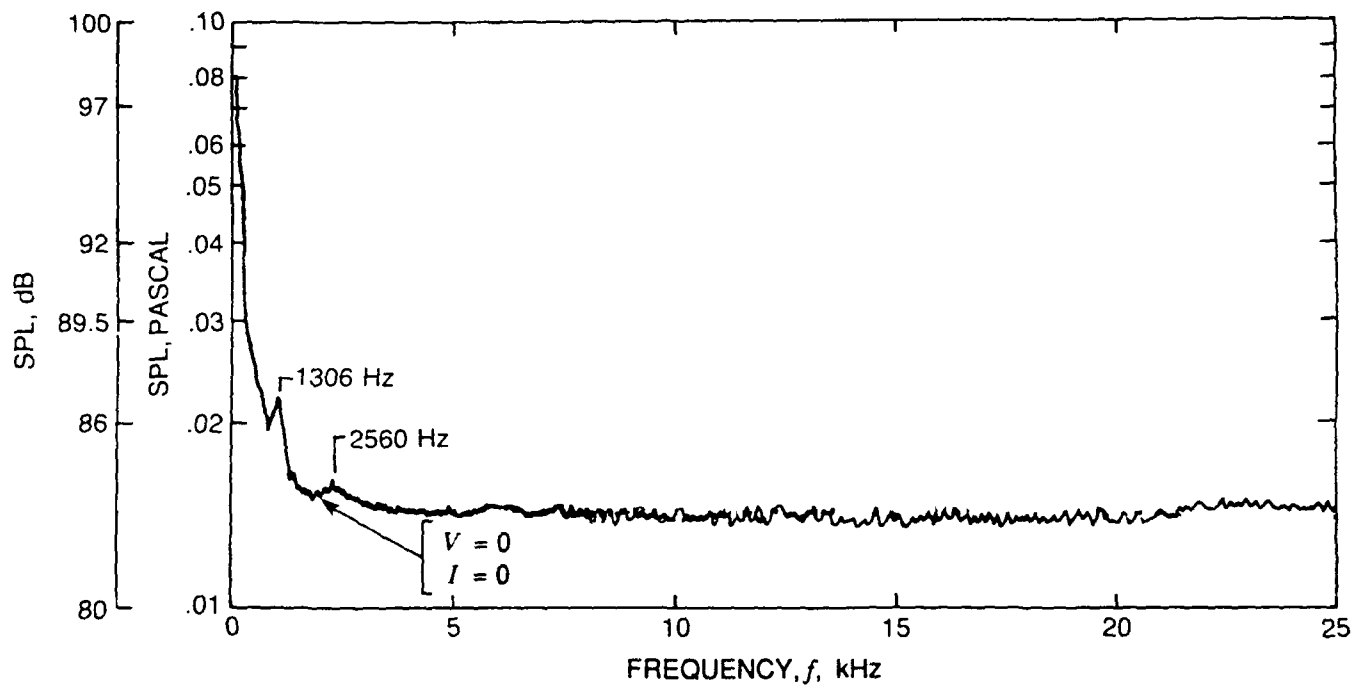
(b) Enclosed channel noise spectra, flow velocity 70 cm/sec.

Fig. 12. Noise spectra in closed channel with no applied voltage and zero current.

(a) $V = 0$, $I = 0$

$w = 5.0$ cm
$d = 1.8$ cm
$l = 12.7$ cm

6200 Hz   34,500 Hz

(b) $V = 12.1$ volts, $I = 2.14$ amp, battery power supply.

2300 Hz

6200 Hz

12,800 Hz

34,500 Hz

(c) $V = 30$ volts, $I = 5.5$ amp, ac/dc power supply.

SOUND PRESSURE LEVEL
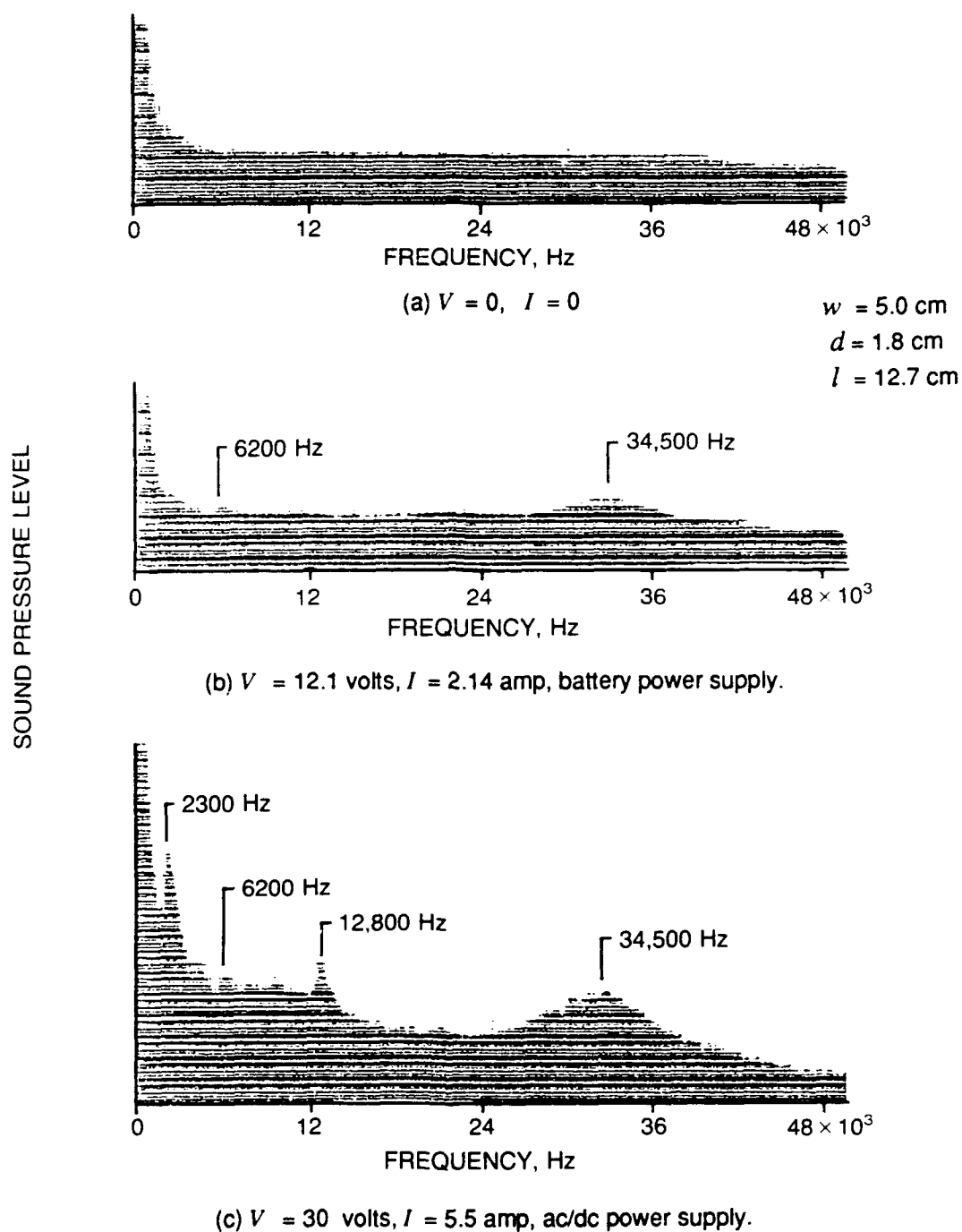
FREQUENCY, Hz

Fig. 13. High frequency noise spectrum with battery and ac/dc power supply; probe was 3 cm downstream.
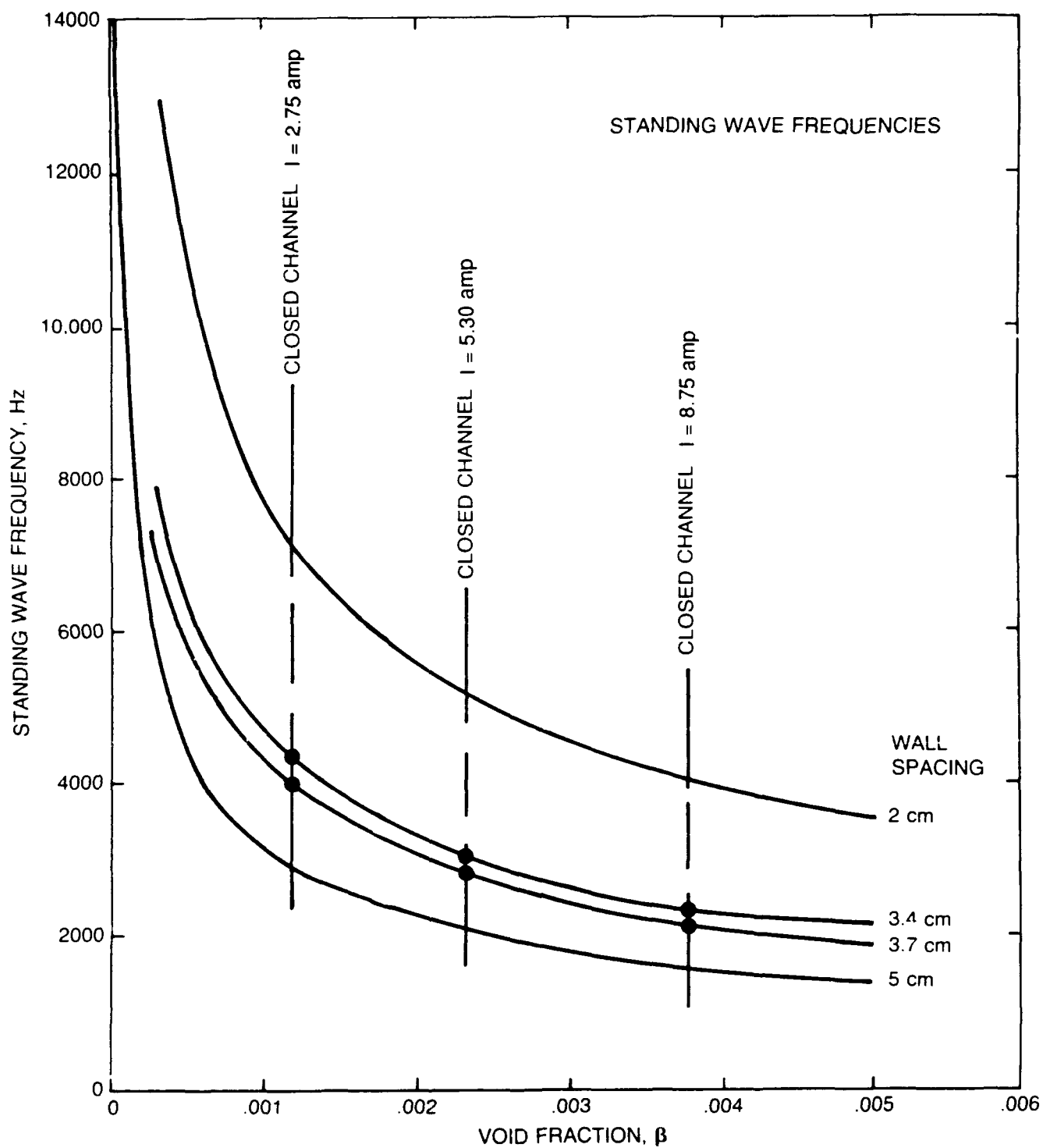
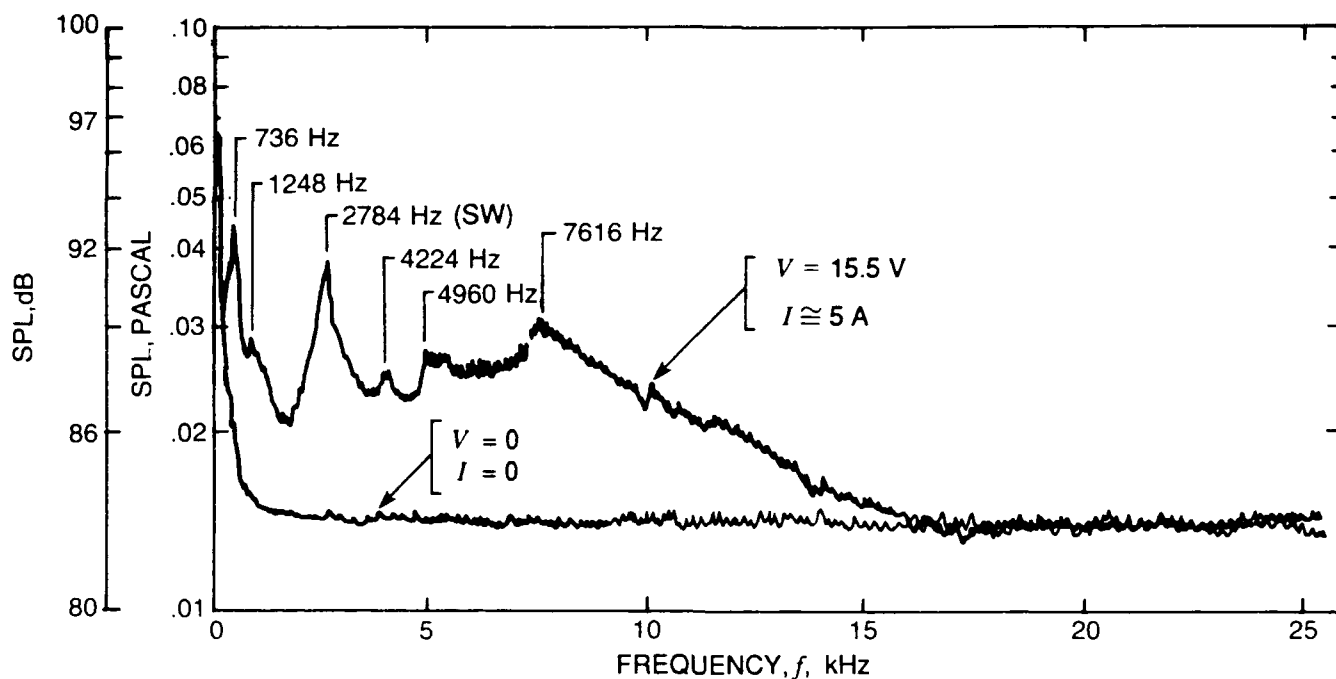**Fig. 14.** Calculated standing wave frequencies at different test conditions; velocity = 26 cm/sec.

$\gamma = c_p/c_v = 1.4$

$p = 1\text{atm}$

DAMPING NEGLECTED
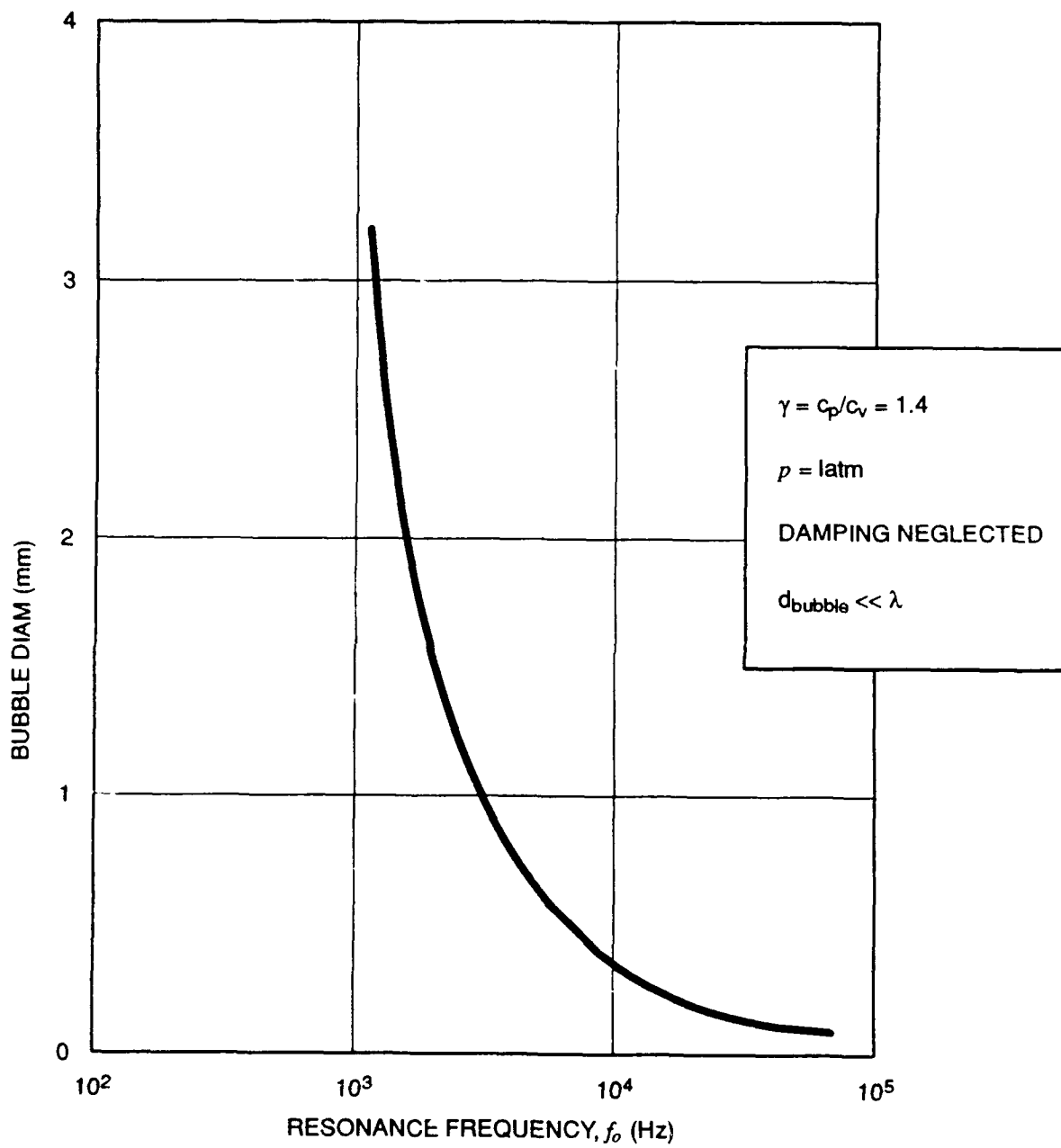
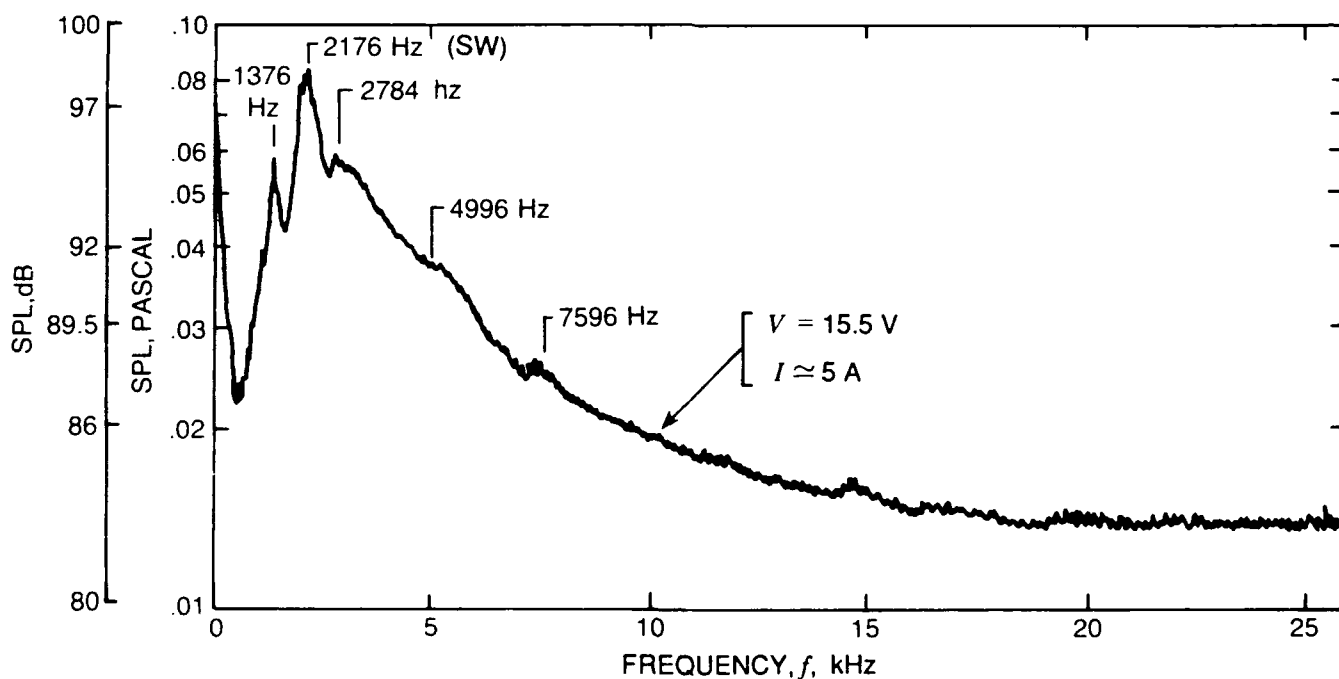$d_{bubble} \ll \lambda$

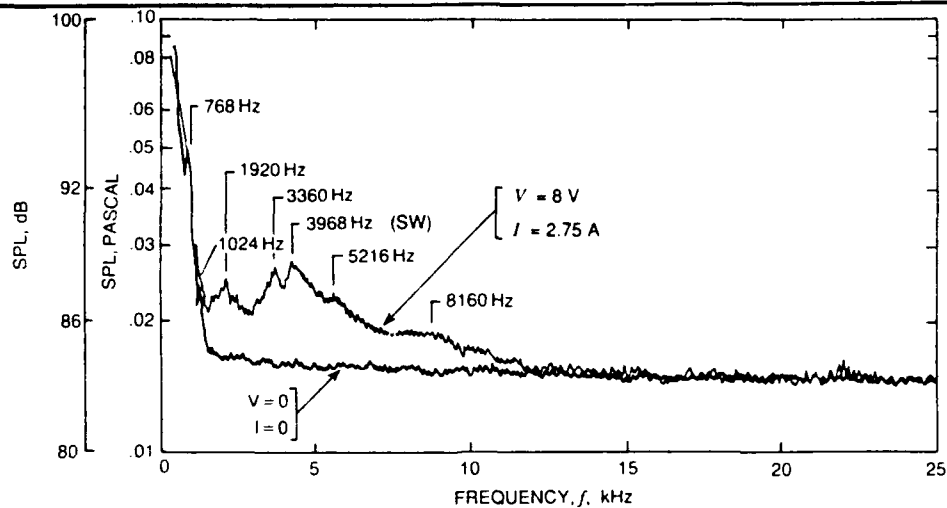**Fig. 15.** Resonance frequency of gas bubbles in water.
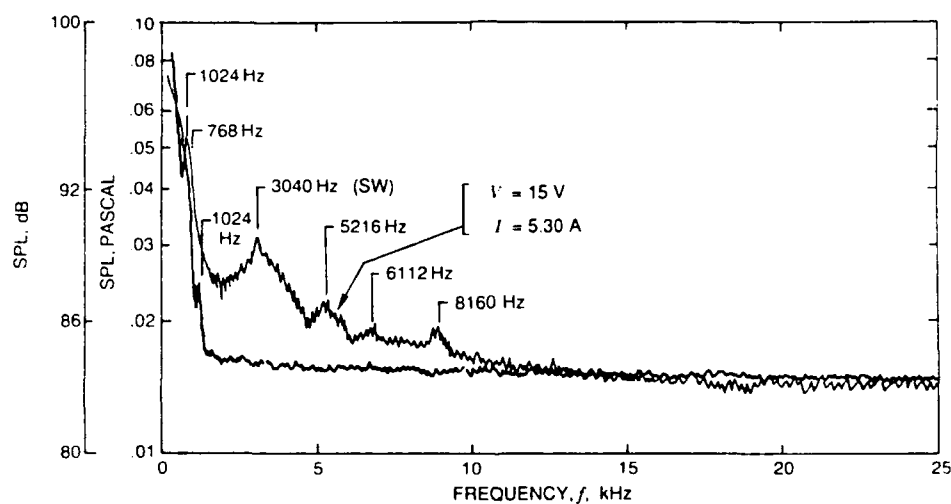
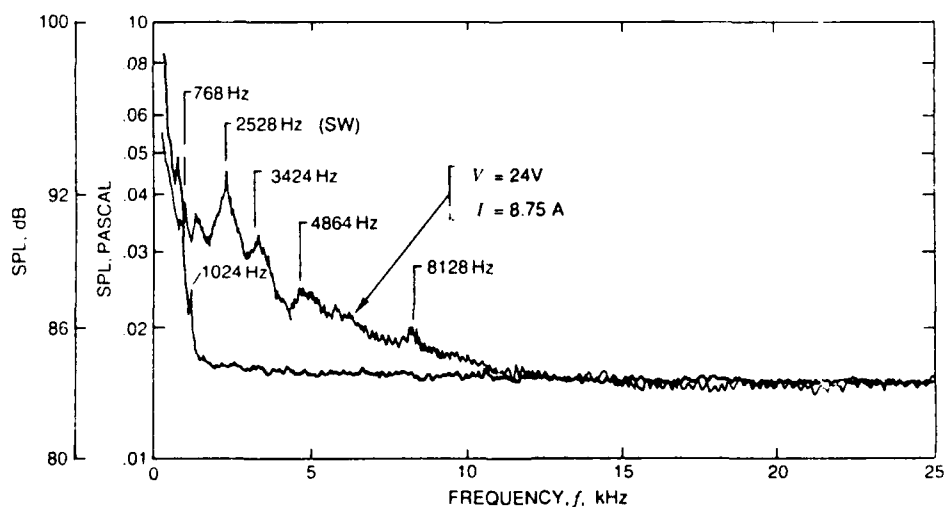(a) Probe 3-cm downstream of channel.

(b) Probe 5-cm upstream of channel.

Fig. 16. Noise spectra for enclosed channel; zero flow velocity and aluminum electrodes.

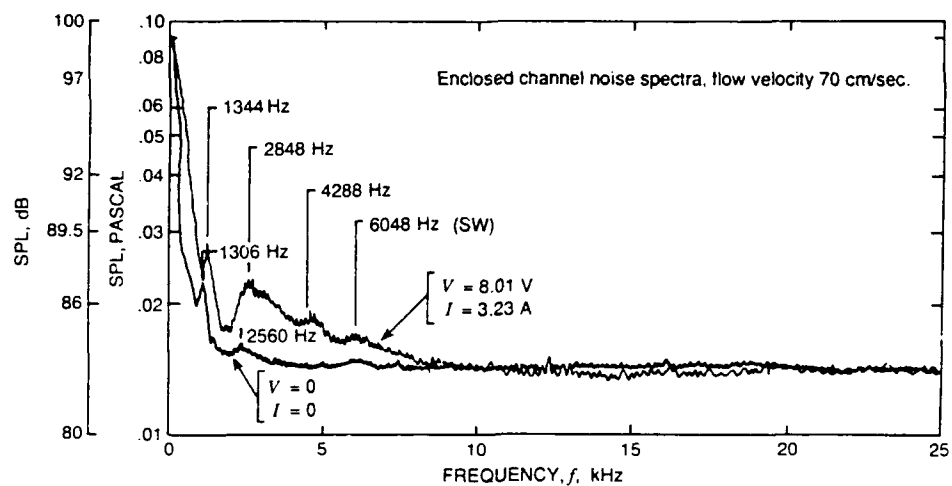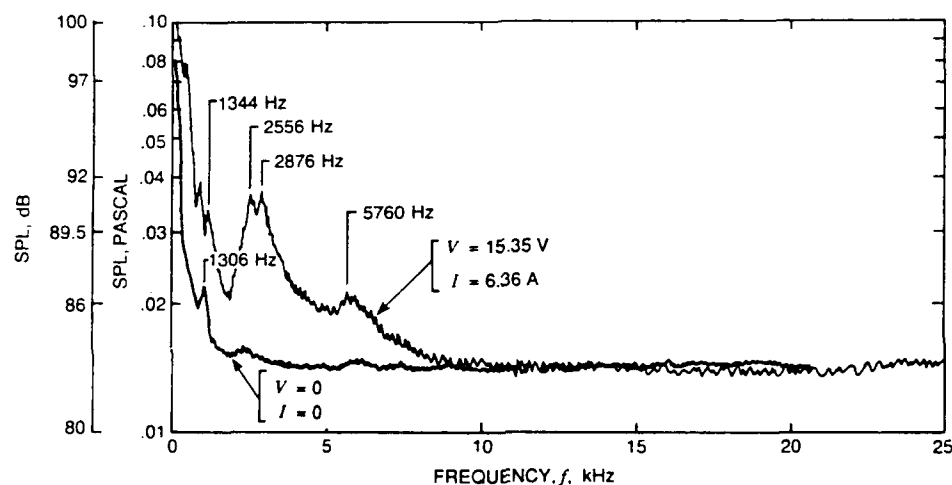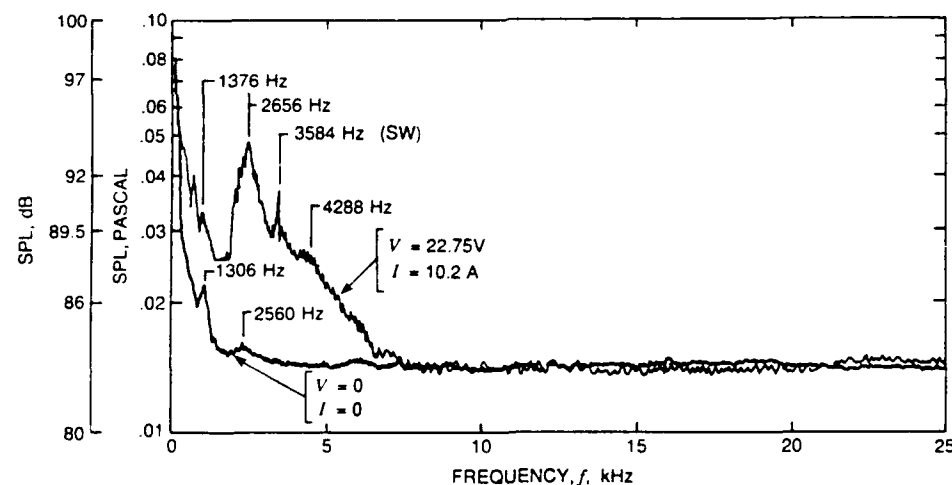**Fig. 17.** Noise spectra for enclosed channel at different test conditions and u_∞ = 26 cm/sec.

(a) Hydrophone 10-cm downstream, V = 8.01 volts.

(b) Hydrophone 10-cm downstream, V = 15.35 volts.

(c) Hydrophone 10-cm downstream, V = 22.75 volts.

Fig. 18. Noise spectra for enclosed channel at different test conditions and u_∞ = 70 cm/sec.
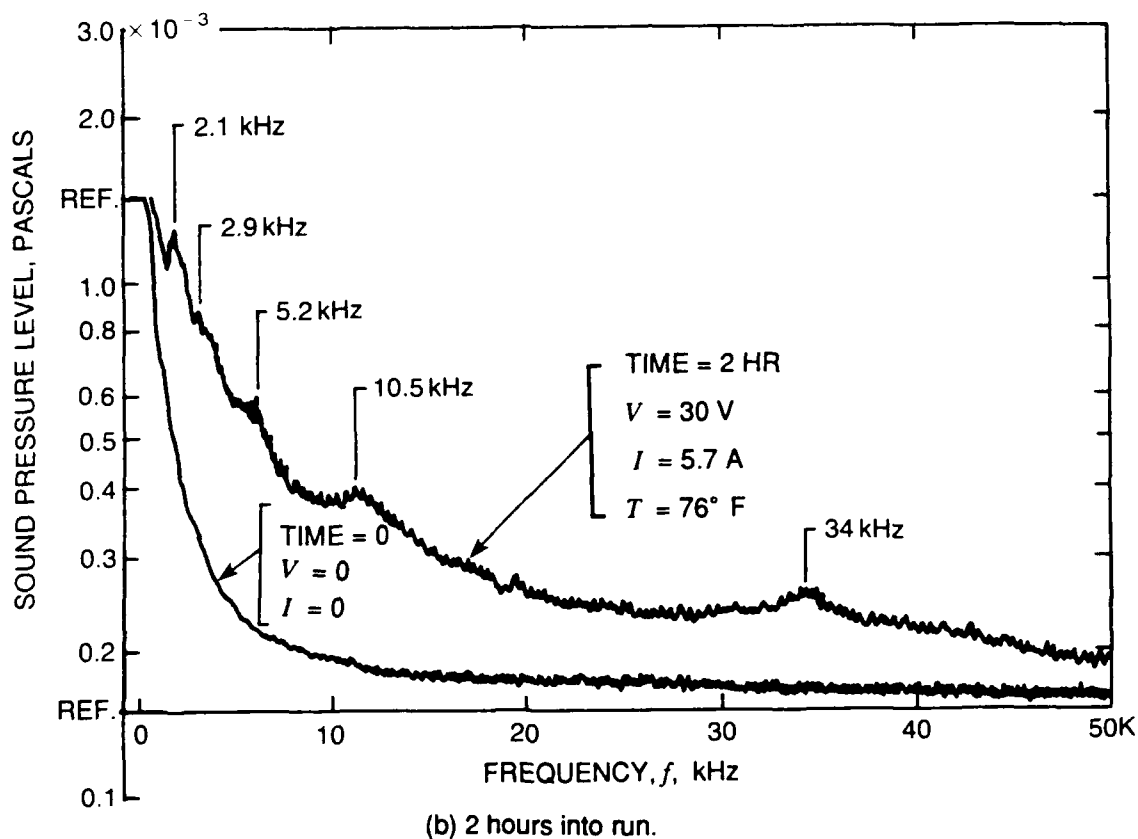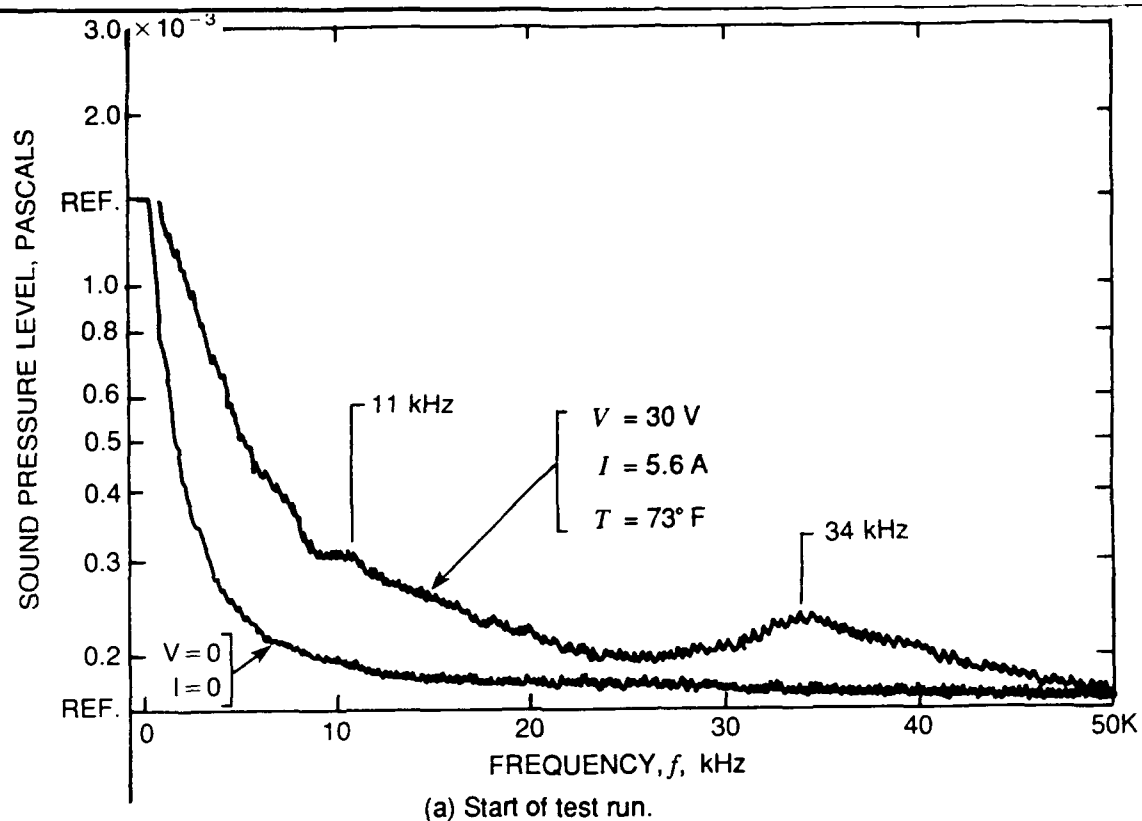
(a) Start of test run.

(b) 2 hours into run.

Fig. 19. Open channel noise spectra showing variation with run time.
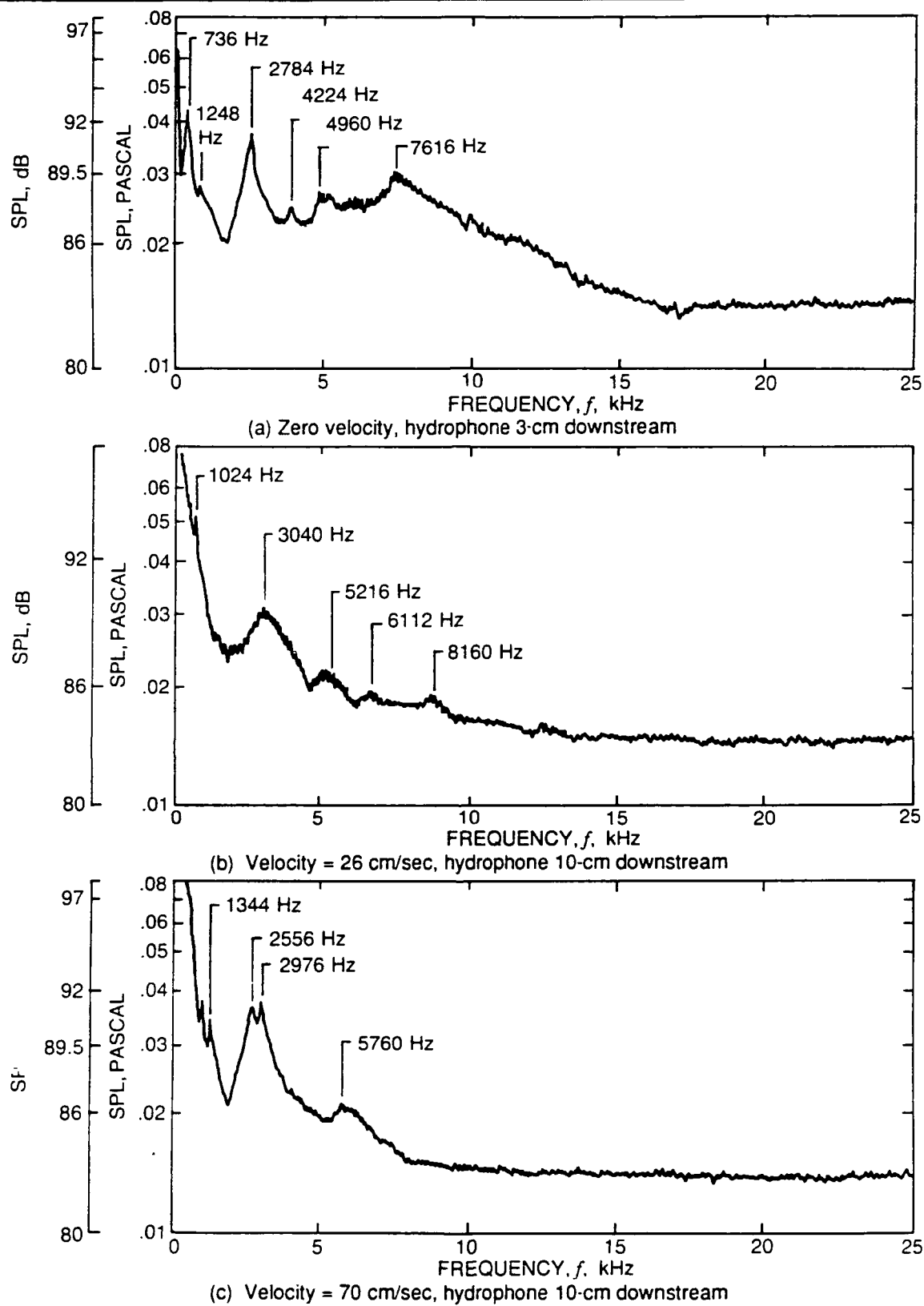
Fig. 20. Effect of flow velocity on noise spectra; applied voltage = 15.5 V.

(a) Zero velocity, hydrophone 3-cm downstream

(b) Velocity = 26 cm/sec, hydrophone 10-cm downstream

(c) Velocity = 70 cm/sec, hydrophone 10-cm downstream

REFERENCES

1. Friauf, James B., "Electromagnetic Ship Propulsion," *ASNE Journal*, pp. 139–142, (Feb 1961).

2. Phillips, Owen M., "The Prospects for Magnetohydrodynamic Ship Propulsion," *Journal of Ship Research*, pp. 43–51 (Mar 1962).

3. Doragh, R.A., "Magnetohydrodynamic Ship Propulsion Using Superconducting-Magnets," Presented at Annual Meeting, Society of Naval Architects and Marine Engineers, New York, N.Y. (Nov 14 & 15, 1963).

4. Way, S., "Propulsion of Submarines by Lorentz Forces in the Surrounding Sea," ASME Publication 64–WA/ENER7, Winter Meeting (Nov 29 – Dec 4, 1964).

5. Hummert, George T., "An Evaluation of Direct Current Electromagnetic Propulsion in Seawater," Office of Naval Research Report ONR–CR168–007–1 (Jul 1979).

6. Way, S., "Electromagnetic Propulsion for Cargo Submarines," *Journal of Hydrodynamics*, Vol. 2, No. 2 (Apr 1968).

7. Hillkirk, John, "Japan Weighing Anchor on 60 mph Freights," *USA Today*, p. 8B, (Mar 2, 1989).

8. Motora, Siezo, S. Takezawa, and H. Tamma, "Research and Development of Superconducting Electro-Magnetic Ships," Technical Report of Tsukuba Institute 9(1) pp. 1–9 (Apr 1989).

9. Corlett, Roy, "Soviet Submarine Propellerless Propulsion — New Developments," *Maritime Defence*, pp. 424–425 (Dec 1987).

10. Corlett, Roy, "The Victor Class: Operational Test Beds for New Generations of Soviet Submarines," *Maritime Defence*, pp. 154–157 (Apr 1985).

11. Bennett, John E., "On-Site Generation of Hypochlorite Solutions by electrolysis of Seawater," *AIChE Symposium Series: Water* (1977).

12. Brown, S.H., J.S. Walker, N.A. Sondergaard, P.J. Reilly, and D.E. Bagley, "Propulsive Efficiencies of Magnetohydrodynamic Submerged Vehicular Propulsors," David Taylor Research Center, DTRC–90/009 (April 1990).

13. Tempelmeyer, Kenneth E., "Electrical Characteristics of a Seawater MHD Thruster," David Taylor Research Center, DTRC–90/017 (Jun 1990).

14. Ross, Donald, *Mechanics of Underwater Noise*, Pergamon Press (1976).

15. Bennett, J.E., "Electrodes ⸍ r Generation of Hydrogen and Oxygen from Seawater," *Int. Journal of Hydrogen Energy*, Vol 5, pp 401–408 (1980).

16. Sides, Paul J., "Phenomena and Effects of Electrolytic Gas Evolution," *Modern Aspects of Electrochemistry*, No. 18, pp. 303–355, Plenum Press (1980).

17. Minnaert, M., "On Musical Air Bubbles and the Sounds of Running Water," *Phil. Magazine*, Vol. 16, pp. 235–248 (1933).

18. Strasberg, M., "Gas Bubbles as Sources of Sound in Liquids," *Journal of the Acoustical Society of America*, Vol. 28, pp. 20–26 (Apr 1956) (Also David Taylor Model Basin Report 1042).

19. Richardson, E.G., Ed., *Technical Aspects of Sound*, Chap. 5 "Air Bubbles in Water," pp. 222–240, Elsevier Publishing Co., New York (1957).

20. Fox, F.F. and K.F. Hertzfeld, *Journal of the Acoustic Society of America*, AM–26, pp. 984–98 (1954).

21. Blouchard, D.C. and A.H. Woodcock, "Bubble Formation and Modification in the Sea," *Tellus*, Vol. 9, No. 2, pp. 147–158 (May 1957).

22. Johnson, B.D. and R.C. Cooke, "Bubble Populations and Spectra in Coastal Waters: A Photographic Approach," *Journal of Geophysical Research*, Vol. 84, No. C7, pp. 3761–3766 (Jul 1979).

23. Johnson, B.D. and R.C. Cooke, "Generation of Stabilized Microbubbles in Seawater," *Science*, Vol. 213, p. 209 (1981).

24. Scott, J.C., "The Role of Salt in Whitecap Persistence," *Deep Sea Research*, Vol. 22, pp. 653–657 (1975).

25. Prosperetti, Andrea and Nan Q. Lu, "Cavitation and Bubble Bursting as Sources of Oceanic Ambient Noise," *Journal of Acoustic Society of America*, Vol. 84, No. 3, pp. 1037–1041 (Sep 1988).

26. Janssen, L.J.J. and J. Hoogland, "The Effect of Electrolytically Evolved Gas Bubbles on the Thickness of the Diffusion Layer," *Electrochemica Acta*, Vol. 18.

INITIAL DISTRIBUTION

Copies

3   DARPA/STP
    LCDR Richard Martin
    Advanced Technology
    1515 Wilson Blvd., Suite 705
    Arlington, VA 22209

3   ONT
    Gene Remmers
    Office of Chief of Naval Research
    Office of Naval Techology
    800 N. Quincy St.
    Arlington, VA 22217-5000

4   NAVSEA
    1   SEA 08
    1   SEA 92R
    2   SEA 55N

12 DTIC

2   Dr. John S. Walker
    University of Illinois at Urbana-
        Champaign
    Dept. Mech. & Ind. Engineering
    144 Mechanical Engineering Bldg.
    1206 West Green St.
    Urbana, Illinois 61801

2   Dr. Daniel W. Swallom
    Avco Research Laboratory
    2385 Revere Beach Parkway
    Everett, MA 02149

2   Dr. Michael Petrick
    Argonne National Laboratory
    9700 South Cass Ave.
    Argonne, IL 60439

20 Dr. Kenneth E. Tempelmeyer
    c/o Office of the Dean College of
        Engineering and Technology
    Southern Illinois University
    Carbondale, Illinois 62901

2   Dr. Basil Picologlou
    Engineering Physics Division
    Argonne National Laboratory
    9700 South Cass Ave.
    Argonne, Illinois 60439

CENTER DISTRIBUTION

Copies	Code	Name
3	01	Richard E. Metry
3	0113	Dr. Bruce E. Douglas
2	154	Justin H. McCarthy
2	1544	Dr. Frank B. Peterson
1	1561	Geoffrey Cox
1	1902	Dr. G. Maidanik
1	1942	Dr. Theodore M. Farabee
2	27	Larry J. Argiro
2	2704	Dr. Earl Quandt, Jr.
2	271	Howard O. Stevens, Jr.
10	2711	David E. Bagley
2	2711	Robert C. Smith
10	2712	Dr. Neal A. Sondergaard
10	2712	Dr. Samuel H. Brown
2	2712	Michael J. Superczmyski
1	272	Timothy J. Doyle
1	2704.1	Dr. J. Dickey
1	2743	Kevin Crouchley
1	2743	David B. Larrabee
1	3411	Margaret L. Knox
1	3421	TIC Carderock
2	3422	TIC Annapolis
10	3432	Reports Control